FACULTY
OF MATHEMATICS
AND PHYSICS
Charles University

MASTER THESIS

Jana Švrčková

A study of dynamically bounded triple systems

Astronomical Institute of Charles University

Supervisor of the master thesis: prof. RNDr. Petr Harmanec, DrSc.

Study programme: Physics

Study branch: Astronomy and Astrophysics

Prague 2023

I declare that I carried out this master thesis independently, and only with the cited sources, literature and other professional sources. It has not been used to obtain another or the same degree.

I understand that my work relates to the rights and obligations under the Act No. 121/2000 Sb., the Copyright Act, as amended, in particular the fact that the Charles University has the right to conclude a license agreement on the use of this work as a school work pursuant to Section 60 subsection 1 of the Copyright Act.

In . . . . date . . . .
                                                                                                    Author's signature

Title: A study of dynamically bounded triple systems

Author: Jana Švrčková

Department: Astronomical Institute of Charles University

Supervisor: prof. RNDr. Petr Harmanec, DrSc., Astronomical Institute of Charles University

Abstract:

Hierarchical triple stars consist of two stars orbiting each other on a close orbit and a third, more distant star. This is the only observed dynamically stable configuration of triple systems. The third star needs to be far enough from the close binary, otherwise the stars start moving chaotically which eventually results in ejecting one of the components out of the system. This condition is described by several criteria of dynamical stability.

HD 152246 is a hierarchical triple star with an eccentricity seemingly too high to be dynamically stable. Using a recently observed set of spectra, I determined more precise and accurate orbital elements of this system. I showed that the eccentricity value is lower and the system does fulfill stability criteria. I also showed that the system is dynamically evolving - the short orbit inclination is changing in time.

δ Cir is a triple system that consist of an eclipsing binary and a more distant third star. Moreover, there are some signs that the third star is also a binary. Using spectra of the system, I calculated a more precise mutual period of the eclipsing binary and the third star as well as its other orbital elements. I also combined spectroscopic and photometric data to determine more precise parameters of the eclipsing binary.

Keywords: multiple systems - orbital elements

Contents

Introduction

This thesis is focused on study of two already known triple star systems. The orbits of these triple stars are changing dynamically. The first system is HD152246. It consists of two hot stars of spectral type O and one colder star, that has not been yet detected in the spectra. The colder star and one of the O-type stars form a binary system with low value of eccentricity and orbital period of 6 days. In addition, this binary star together with the second O-type star orbit around a common centre of gravity with a period of 470 days. This orbit has the semimajor axis of 10 au and very high value of eccentricity.

The published eccentricity of the mutual orbit of the close binary and the third star is too high. With this value of eccentricity, the system should not be dynamically stable. In my work I will use recently measured spectra from spectrograph CHIRON that are covering mostly a time interval around periastron passage of the system. I will revise the value of eccentricity and try to calculate a more accurate value not only for eccentricity but for other orbital elements as well. I will also try to find out whether the mutual interaction between the system's components causes measurable changes of the orbital elements.

The second triple system δ Cir is formed by three OB stars. Two of them form an eclipsing binary system with orbital period of 3.9 days and a low value of eccentricity. This binary is bounded with the third body in an eccentric orbit. The estimated period of this orbit is 1644 days. There is also a possibility that the third star is actually a binary star as well. The line of apsides of the eclipsing binary rotates with an estimated period of 141 years.

I will analyse recently measured spectra from spectrograph CHIRON together with older spectra from spectrographs UVES, HARPS and FEROS. My goal is to find a more precise value of the period for the mutual orbit of the eclipsing binary and the third star. Then I will calculate more precise orbital elements from using both the above mentioned spectra and several light curves of the eclipsing binary.

The following abbreviations are used in this thesis:

- HJD - heliocentric Julian date

- RJD - reduced Julian date, $RJD = HJD - 2400000.0$

- RV - radial velocity

1. O-type stars

O-type stars are white-blue, hot stars of spectral type O. These stars are very rare, but they can be observed at large distances because of their very high brightness. Less than 0.1% of stellar population is of spectral type O, as was shown by Ledrew [2001]. Most of the known O-type stars in our galaxy are located near the galactic plane.

These stars are also often found in multiple star systems. Spectroscopic surveys show that more than half of O-stars in our Galaxy are part of a binary or multiple stellar systems [Sana, 2017].

The effective temperature of O-stars on the main sequence is usually from $31\,900\,\mathrm{K}$ (O9.5 V) to $44\,900\,\mathrm{K}$ (O3 V). The values of their masses are in the interval from around 15 $M_\odot$ (O9.5 V) to 60 $M_\odot$ (O3 V). Their radii are from 7 $R_\odot$ up to 14 $R_\odot$ [Martins et al., 2005].

The luminosity of massive main sequence stars follows the mass-luminosity relation

$$\frac{L}{L_\odot} = \left(\frac{M}{M_\odot} \right)^{2.76} \tag{1.1}$$

where M is the mass of a star and L is its luminosity, $M_\odot$ is the solar mass and $L_\odot$ is the solar luminosity. This relation holds for stars with masses between 5 $M_\odot$ and 50 $M_\odot$ [Vitrichenko et al., 2007].

Spectra of O-type stars are characterised by the lines of ionized atoms such as He I, He II, CIII, NIII, OIII, SiV. The spectral lines of HI are weak [Karttunen et al., 2007].

Due to their high luminosity, O-stars spend a much shorter time on the main sequence than lower mass stars. Their typical lifetime is only a few million years. Few O-type stars are detected close to zero age main sequence on the HR diagram, this holds true also for large samples without observational bias [Holgado et al., 2020].

2. Binary and multiple star systems

2.1 Binary stars

The simplest model of a binary star consists of two isolated point masses which interact through Newtonian gravitation. The larger is the separation between the stars, the better this approximation works.

According to the solution of two body problem, both stars revolve around each other on elliptical orbits. The centre of mass is located in common focus of these ellipses. The orbits are sketched in Figure 2.1. The primary (more massive) star with mass M_1 moves on an elliptical orbit with semi-major axis a_1. Semi-major axis of the secondary star with mass M_2 is a_2. Both orbits have the same eccentricity $e_1 = e_2$. Using the formula for centre of mass, we obtain a relation between the mass ratio and semi-major axis ratio of the binary

$$\frac{a_1}{a_2} = \frac{M_2}{M_1} \tag{2.1}$$

We denote P the orbital period of the binary and G the gravitational constant. Then the third Kepler's law is

$$P^2 = \frac{4\pi^2 a^3}{G(M_1 + M_2)} \tag{2.2}$$

where a is semi-major axis of relative orbit, which we get if the primary star is located in the origin of the coordinate system. It is the sum of a_1 and a_2

$$a = a_1 + a_2 \tag{2.3}$$

The minimal and maximal distance of the binary components is

$$r_{\min} = a(1 - e) \tag{2.4}$$

$$r_{\max} = a(1 + e) \tag{2.5}$$

where e is numerical eccentricity of the orbit.

Semi-major axis and eccentricity determine the size and shape of the orbit. Orientation of the orbit in space is described by another three angular elements. Inclination i is the angle between the plane of the orbit and the plane of the sky. Longitude of periastron ω_{p} is the angle between the ascending node and the periastron. Periastron longitude of the primary component differs by 180° from the periastron longitude of the secondary, $\omega_{\mathrm{p2}} = \omega_{\mathrm{p1}} + 180°$. Longitude of the node Ω is position angle of the line of nodes. Orientation of an orbit is sketched in Figure 2.2.

If the primary star is in the origin of the coordinate system then the position of the secondary star is described by polar coordinates (r, v)

$$r = \frac{a(1 - e^2)}{1 + e \cos v} \tag{2.6}$$
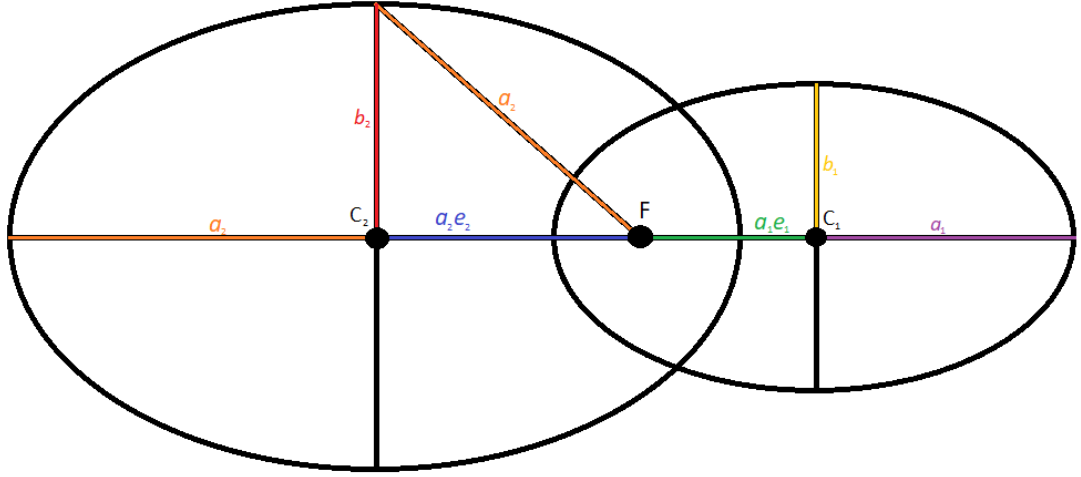
Figure 2.1: Orbital elements of a binary star
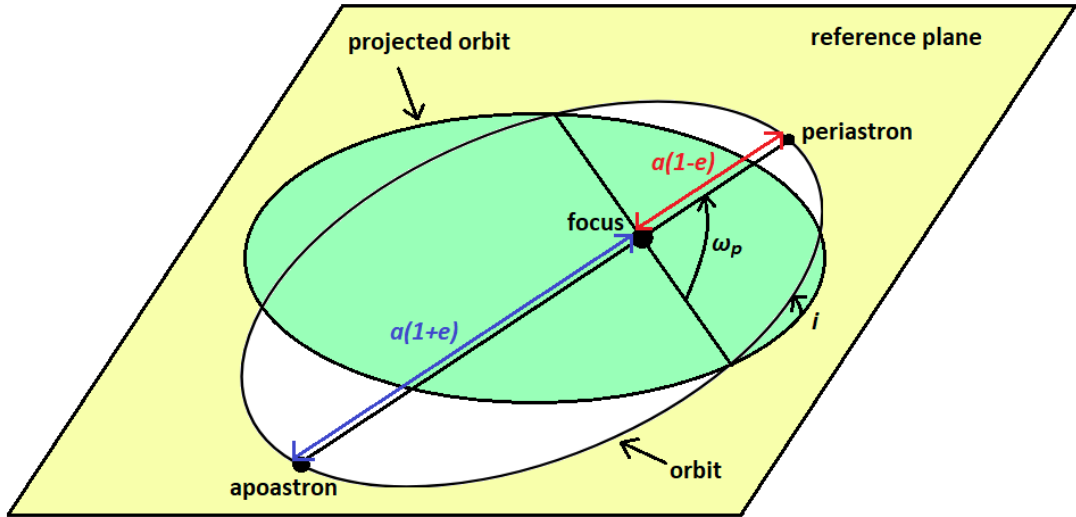
Figure 2.2: Orbital elements of a binary star

The angular coordinate v is called true anomaly, a is the semi-major axis and e is the eccentricity of the relative orbit.

The position of the secondary star in the relative orbit is given by true (v), mean (M) or eccentric anomaly (E). The mean anomaly describes position of the secondary star as if it moved on a circular orbit

$$M = 2\pi \frac{t - T_{\mathrm{p}}}{P} \qquad (2.7)$$

The true anomaly v is related to the eccentric anomaly E

$$\tan \frac{v}{2} = \sqrt{\frac{1+e}{1-e}} \tan \frac{E}{2} \qquad (2.8)$$

Eccentric anomaly E and mean anomaly M are related via the Kepler equation

$$E = M + e \sin E \qquad (2.9)$$

Eccentric anomaly has to be solved numerically, because the Kepler equation is transcendental. Figure 2.3 shows all three anomalies of a secondary star located at point S. The primary star is located at the focus F, the letters P, A and C denote positions of periastron, apoastron and the centre of the ellipse.
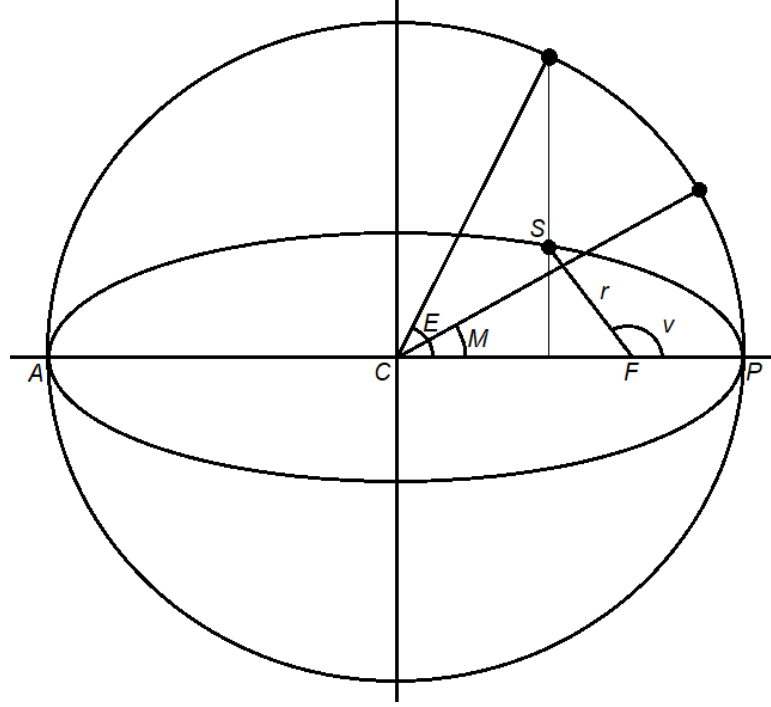
Figure 2.3: Position in the orbit - mean, eccentric and true anomaly.

The orbital motion of the stars causes periodical changes of wavelength of the spectral lines. Using the formula for Doppler shift, we can measure radial velocities (velocities parallel to the line of sight) of the stars

$$\frac{RV}{c} = \frac{\Delta\lambda}{\lambda_0} \qquad (2.10)$$

Radial velocity as a function of time can be derived from equations 2.6 to 2.9 and from the geometry of the orbit. The result is

$$RV_1 = \gamma + K_1(\cos(\omega_{p1} + v(t)) + e \cos\omega_{p1}) \qquad (2.11)$$

$$RV_2 = \gamma - K_2(\cos(\omega_{p2} + v(t)) + e \cos\omega_{p2}) \qquad (2.12)$$

where K_1 and K_2 are semi-amplitudes of radial velocity and γ is radial velocity of the centre of mass. The following equations hold for the semi-amplitudes of radial velocity

$$a_1 \sin i = \frac{P}{2\pi} K_1 \sqrt{1 - e^2} \qquad (2.13)$$

$$a_2 \sin i = \frac{P}{2\pi} K_2 \sqrt{1 - e^2} \qquad (2.14)$$

Dividing these last two equations and using 2.1, we obtain

$$\frac{a_1}{a_2} = \frac{K_1}{K_2} = \frac{M_2}{M_1} \tag{2.15}$$

In case we are just able to observe spectrum of the brighter star, we can determine only $a_1 \sin i$ (if the primary star is also the brighter one) and a quantity called mass function $f(M)$

$$f_1(M) = \frac{K_1^3}{2\pi G} P(1 - e^2)^{\frac{3}{2}} = \frac{q^3}{(1+q)^2} M_1 \sin^3 i \tag{2.16}$$

2.1.1 Apsidal advance

In an ideal case when the two components of an eccentric binary are just point masses, their Keplerian orbit does not change in time. In reality, the stars have finite volume and a non-spherical shape. The mass distribution causes rotation of the apsidal line in the direction of orbital motion. The process is described by the rate of change $\dot{\omega}_{\mathrm{p}}$ of the periastron longitude. In general $\dot{\omega}_{\mathrm{p}}$ is a sum of two terms, one relativistic and one Newtonian due to the mass distribution of the stars

$$\dot{\omega}_{\mathrm{p}} = \dot{\omega}_{\mathrm{R}} + \dot{\omega}_{\mathrm{N}} \tag{2.17}$$

The relativistic term is (Levi-Civita [1937], Robertson [1938])

$$\dot{\omega}_{\mathrm{R}} = \frac{6\pi G}{c^2} \frac{M_1 + M_2}{Pa(1 - e^2)} \tag{2.18}$$

The classical term is [Sterne, 1939]

$$\begin{aligned}
\dot{\omega}_{\mathrm{N}} = &\frac{2\pi}{P} k_{2,1} \frac{R_1^5}{a^5} \left[15 \frac{m_2}{m_1} f(e) + \frac{\omega_1^2}{m_1} \frac{a^3}{G} g(e) \right] \\
&+ \frac{2\pi}{P} k_{2,2} \frac{R_2^5}{a^5} \left[15 \frac{m_1}{m_2} f(e) + \frac{\omega_2^2}{m_2} \frac{a^3}{G} g(e) \right]
\end{aligned} \tag{2.19}$$

where R_1 and R_2 are mean radii of the stars, $k_{2,1}$ and $k_{2,2}$ are constants of their inner structure. They are equal to 0.75 for a homogeneous sphere and equal to 0 for a point mass. The functions of eccentricity are

$$f(e) = 1 + \frac{13}{2} e^2 + \frac{181}{8} e^4 + \frac{465}{8} e^6 + \dots \tag{2.20}$$

$$g(e) = 1 + 2e^2 + 3e^4 + 4e^6 + \dots \tag{2.21}$$

When dealing with the apsidal advance, it is necessary to take into account the difference between two types of orbital period. The sidereal orbital period P_{sid} is determined with respect to the stars while the anomalistic period P_{a} is the time interval between two subsequent passages through periastron. The anomalistic and sidereal period are connected through the following equation

$$P_{\mathrm{sid}} = \left(1 - \frac{\dot{\omega}_{\mathrm{p}}}{2\pi} \right) P_{\mathrm{a}} \tag{2.22}$$

2.2 Triple-star systems

Multiple star systems occur in two configurations. In the so-called trapezia (named after Trapezium in Orion), the distances between all the components of the system are comparable. These systems are dynamically unstable and short-lived. Due to that, the chance of finding a trapezium system with stars on the main sequence is very low. Several known trapezia candidates are formed by pre-main sequence stars [Tokovinin, 2021].

The other configuration is called hierarchical. Such systems can be described as a hierarchical combination of binary stars. The separations between the objects in various levels of hierarchy are significantly different.

Hierarchical triple system consists of two close stars that form so called inner binary and a more distant third star. The distance of the third component from the inner binary is significantly larger than the distance between the two components of the inner binary. The mutual orbit of the third body and the inner binary is called the outer orbit. A sketch of a hierarchical triple star is in Figure 2.4.

Hierarchical systems are quite common in the solar neighbourhood. Roughly 17% of solar-type stars within the distance of 67 pc are part of a hierarchical system [Tokovinin, 2014]. This holds true also for a small but well studied sample of stars within the distance of 25 pc [Hirsch et al., 2021].
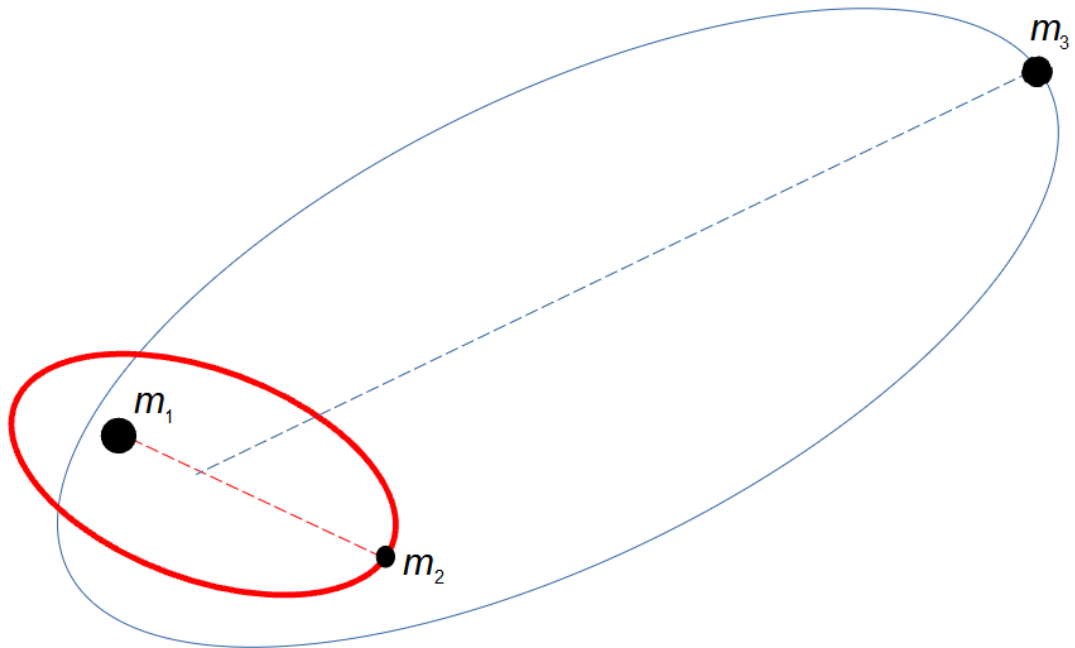
Figure 2.4: Schematic drawing of a hierarchical triple star system.

A hierarchical triple system can be described by two sets of orbital elements that are mentioned in the section about binary stars. One of the sets describes the inner orbit the second set describes the outer orbit. In addition to these elements, two more parameters are used. The first one is the mutual inclination of the inner and outer orbit. The second parameter is the ratio of inner and

outer orbital period P_{out}/P_{in}. In general, the elements of inner and outer orbit can change in time due to dynamical interaction between the components of the triple system.

If the masses of the stars are denoted m_1 for primary, m_2 for secondary and m_3 for third star, then the mass ratio of the inner binary is

$$q_{in} = \frac{m_2}{m_1} \qquad (2.23)$$

The mass ratio of the outer binary is defined analogically

$$q_{out} = \frac{m_3}{m_1 + m_2} \qquad (2.24)$$

The semi-amplitudes of radial velocity can be determined from spectroscopic data. Because the ratio of RV semi-amplitudes is the inverted mass ratio, the following relations hold

$$q_{in} = \frac{m_2}{m_1} = \frac{K_1}{K_2} \qquad (2.25)$$

$$q_{out} = \frac{m_3}{m_1 + m_2} = \frac{K_{1+2}}{K_3} \qquad (2.26)$$

where K_1, K_2 and K_3 are the semi-amplitudes of radial velocity of the primary, secondary and third star, respectively. K_{1+2} is the RV semi-amplitude of the inner binary's center of mass.

2.2.1 Dynamical stability of triple-star systems

As was already said in the previous section, dynamically stable multiple star systems are hierarchical. If a hierarchical system is dynamically unstable, its hierarchy will eventually break and the stars begin to move chaotically. The chaotic movement eventually results in ejecting one of the stars out of the system - usually it is the least massive one.

The dynamical stability of a hierarchical system depends on the distances between the components. If the third star moves on its orbit too close to the inner binary, the system is unstable. There were several attempts to find a criterion of dynamical stability. A theoretical stability limit was derived by Mardling and Aarseth [2001]

$$\frac{P_{out}}{P_{in}} \geq 4.7(1 + q_{out})^{1/10} \frac{(1 + e_{out})^{3/5}}{(1 - e_{out})^s} \qquad (2.27)$$

where the value of the parameter s is 1.8. This limit was later improved by Sterzik and Tokovinin [2002], who showed that according to numerical simulations a better value of the exponent is $s = 1.35$. They deemed a system dynamically stable if it stayed hierarchical in numerical simulations for 300 crossing times.

Tokovinin [2004], Tokovinin [2007] showed that 38 systems with $P_{out} < 300\,\mathrm{yr}$ satisfy an empirical stability criterion

$$\frac{P_{out}}{P_{in}}(1 - e_{out})^3 \geq 5 \qquad (2.28)$$

Borkovits et al. [2016] analysed eclipsing binaries discovered in the Kepler field. They studied light-travel-time effect (LTTE) or dynamical effect delays

of eclipse timing and found indication for a third body in 222 systems. Not all of these systems fulfill the empirical stability criterion 2.28, but they fulfill the criterion 2.27 with $s = 1.8$ derived by Sterzik and Tokovinin [2002]. This means that the empirical criterion might be caused just by some observational effect.

Figure 2.5 shows eccentricity of the outer orbit as a function of period ratio $P_{\text{out}}/P_{\text{in}}$. 310 triple star systems are plotted there together with the three mentioned stability criteria.
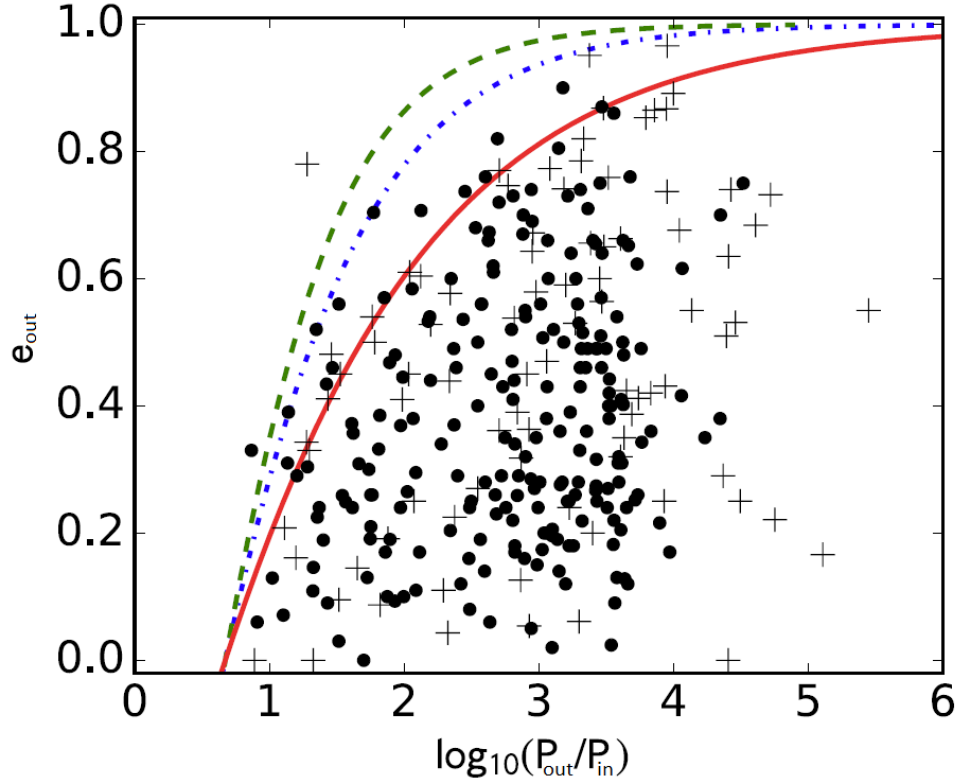
Figure 2.5: Plot of the outer orbit eccentricity vs. the ratio of outer and inner orbital period. 222 Kepler triples are plotted with dots [Borkovits et al., 2016] and 88 triple stars from Multiple Star Catalog [Tokovinin, 2018] are plotted with crosses. The empirical stability criterion 2.28 is plotted with red solid line, theoretical criterion 2.27 with $s = 1.8$ is plotted with blue dash-dotted line and green dashed line is 2.27 with $s = 1.35$. Image credit: [Juryšek et al., 2018]

3. HD 152246

HD 152246 (HIP 82685) is a hierarchical triple-star system that consists of two hot stars of spectral type O and one colder star that has not yet been detected in the spectra. It is a member of the Sco OB1 association. One of the O-type stars forms a close binary together with the colder star. The period of this inner orbit is about 6 days and the eccentricity of the orbit is low. The binary and the second O-star revolve around each other in an outer orbit with a high value of eccentricity and orbital period of about 470 days [Nasseri et al., 2014].

Thackeray et al. [1973] first discovered that HD 152246 is a spectroscopic binary. In 1963-1967 they measured 6 radial velocities in range from $-58\,\mathrm{km/s}$ to $60\,\mathrm{km/s}$. They classified the star as O8.5 III.

Conti et al. [1977] published one more value of radial velocity and also noted that the object is a binary star.

Stickland and Lloyd [2001] discovered sharp and wide lines in the spectra and published two values of radial velocities for both components. They also determined the projections of their rotational velocities as $59\,\mathrm{km/s}$ and $156\,\mathrm{km/s}$.

Spectral classification of this object was done in many other works. Morgan et al. [1955] first classified the object as O9 III. Schild et al. [1969] and Garrison et al. [1977] later got the same result, while Walborn [1973] classified the system as O9 III-IV(n). Finally, Sota et al. [2014] and Maíz Apellániz et al. [2016] assigned spectral type of O9 IV.

The visual magnitude determined in several works is: $V = 7.31$ [Thackeray et al., 1973], $V = 7.35$ [Klare and Neckel, 1977], $V = 7.33$ [Dachs et al., 1982] $V = 7.31$ [Schild et al., 1983], $V = 7.35$ [Høg et al., 2000] and $V = 7.29$ [Ducati, 2002].

Paunzen [2015] included HD 152246 in a catalogue of Strömgren-Crawford uvbyβ photometry. There exist also two photometry segments obtained by the TESS space telescope.

Astrometric measurements of the system are listed in Table 3.1. The published radial velocities mentioned above are in Table 3.2.

Fossati et al. [2015] did spectropolarimetric measurements of several OB stars and they did not detected magnetic field of this system. However, according to newest spectropolarimetric observations, HD 152246 definitely has a magnetic field [Hubrig et al., 2023]. It is possible that it belongs to the more distant (and faster rotating) third star.

Table 3.1: Astrometry of HD152246 [Gaia Collaboration, 2022].

Right ascension (J2016)	$\alpha = 16^{\mathrm{h}}\,54^{\mathrm{m}}\,5.297^{\mathrm{s}}$
Declination (J2016)	$\delta = -41°4'46.143''$
Parallax	$p = (0.53 \pm 0.03)$ mas
Proper motion in α	$\mu_\alpha = (-0.51 \pm 0.04)$ mas/yr
Proper motion in δ	$\mu_\delta = (-1.61 \pm 0.03)$ mas/yr

In a study focused solely on HD 152246, Nasseri et al. [2014] analysed 49 spectra from the BESO and FEROS spectrographs. They found that the object

Table 3.2: Published radial velocities of HD 152246. Index 1 refers to RVs measured on the sharp spectral lines, index 3 to RVs measured on the wide spectral lines.

RJD	RV_1	RV_3	Source
38 251.2378	36.0	-	Thackeray et al. [1973]
39 200.6408	60.0	-	Thackeray et al. [1973]
39 200.6498	52.0	-	Thackeray et al. [1973]
39 688.3284	-18.0	-	Thackeray et al. [1973]
39 720.2631	-58.0	-	Thackeray et al. [1973]
39 723.2539	50.0	-	Thackeray et al. [1973]
42 888.780	-29.8	-	Conti et al. [1977]
44 995.778	46.6	-109.4	Stickland and Lloyd [2001]
45 000.609	26.5	-103.0	Stickland and Lloyd [2001]

is a hierarchical triple system where the close inner pair consists of an O-type star (star 1) and one cooler star (star 2). The third, more distant star 3, is an O-type star as well. Orbital period of the inner binary (stars 1 and 2) is $P_\mathrm{in} = (6.004865 \pm 0.000071)$ d, period of the outer orbit is $P_\mathrm{out} = (470.69 \pm 0.48)$ d.

Their solutions of orbital elements obtained from program KOREL are listed in Table 3.3. Using KOREL, they tried to disentangle all three of the spectra, but they could not detect any weak lines from the cooler star 2. They concluded that star 2 has a much lower mass than star 1.

Combining the spectroscopic data together with 3 measurements from the PIONIER interferometer they derived a three-dimensional solution of the outer orbit. Inclination of the orbit was constrained to $i = 112.46^{+6.98}_{-9.11}{}^\circ$ and the semi-major axis to $a = (4.15 \pm 0.15)$ au. This allowed them to calculate masses of the components: $M_{1+2} = (22.78 \pm 1.82)$ M$_\odot$, $M_3 = (20.35 \pm 1.50)$ M$_\odot$.

The disentangled spectra were compared to synthetic spectra. Based on the fit, they estimated the effective temperature of component 1 as $T_{\mathrm{eff},1} = (33\,600 \pm 600)$ K. Projection of rotational velocity is $v_1 \sin i = (65 \pm 3)$ km.s^{-1}. Spectral type of star 1 is O9 V.

Component 3 is an O9 IV star with effective temperature $T_{\mathrm{eff},3} = (33\,000 \pm 500)$ K and projected rotational velocity $v_3 \sin i = (210 \pm 10)$ km.s^{-1}.

Table 3.3: KOREL solutions for orbital elements of HD152246 [Nasseri et al., 2014]

Short orbit	
T_p (RJD)	$54\,285.344 \pm 0.025$
e	0.1122 ± 0.0001
ω_p (°)	$3\,50.4 \pm 0.8$
K_1 (km.s^{-1})	34.60 ± 0.68
Long orbit	
T_p (RJD)	$54\,981.86 \pm 0.11$
e	0.865 ± 0.002
ω_p (°)	123.3 ± 0.12
K_3 (km.s^{-1})	93.2 ± 0.8
q	0.8964 ± 0.0044
K_{1+2} (km.s^{-1})	83.6 ± 1.0

According to the stability criterion 2.27, this system should not be dynamically stable. The value of eccentricity of the outer orbit is too high and the stability criterion is fulfilled for neither value of coefficient s.

It is still possible that the outer eccentricity is actually lower. To determine a precise value of eccentricity from RV curve the periastron passage must be sufficiently covered by RV measurements. If there are no data close to the periastron passage then the shape of RV curve can not be determined precisely. Thus the values of eccentricity and semi-amplitude of RV are not reliable enough. Figure 3.1 shows that there were no RV measurements close to the peak of RV curve.

Moreover the BESO and FEROS spectra covered several 470-d orbital periods. During that time some of the orbital elements could change which would skew the results even more.

It is thus necessary to obtain new spectra covering a time interval around the periastron passage. These spectra were obtained during 2021 and 2022. The time of periastron passage in the 470-day orbit was predicted for April 12, 2022.

3.1 Origin of the spectra

215 of the spectra used in this thesis originate from CHIRON spectrograph located in Cerro Tololo Inter-American Observatory (CTIO). CHIRON is a cross-dispersed echelle spectrograph fed by fiber. It is used at the SMARTS 1.5-meter telescope, which is an open-tube Cassegrain. The spectrograph is highly stable and is used mainly for precise measurements of radial velocities. Depending on the mode, three spectral resolutions are possible: $R \sim 25\,000$, $R \sim 80\,000$ and $R \sim 140\,000$.

The spectra cover two time intervals, the first one is from RJD 59 280 to RJD 59 492 (from March to October 2021). The second time interval is from RJD 59 652 to RJD 59 859 (from March to October 2022). Their resolution is $R \sim 25000$ (the spectrograph was in fiber mode). Wavelength range of the spectra is
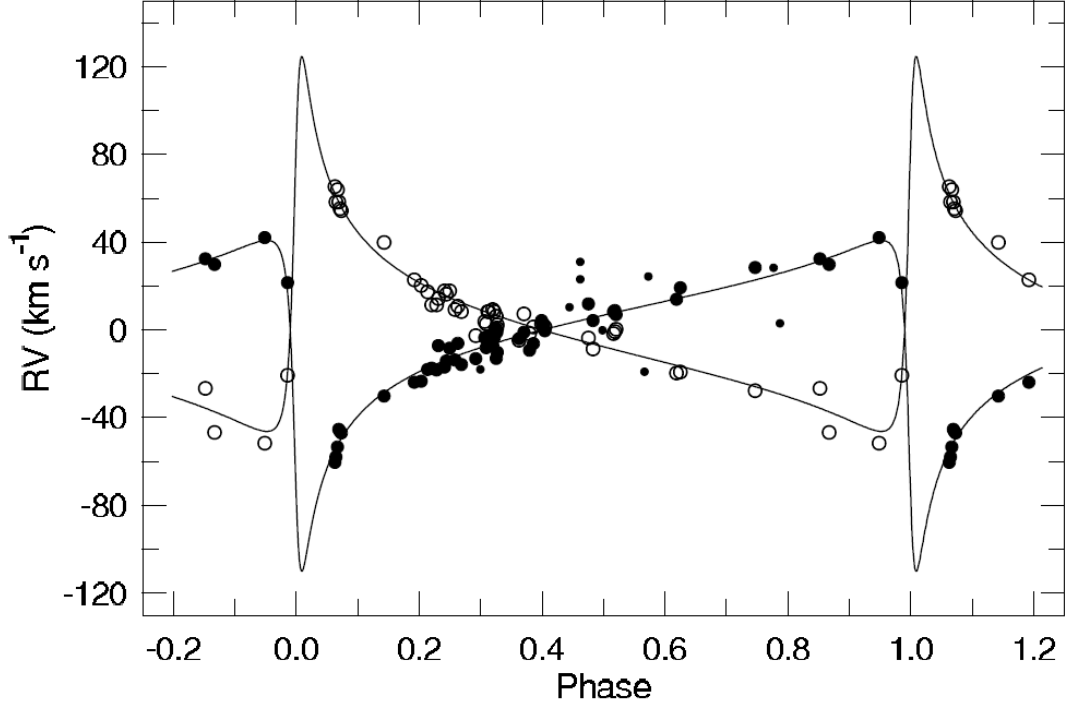
Figure 3.1: RV curve of stars 1 and 3 in the outer orbit. Most of RVs were measured on BESO and FEROS spectra, the rest comes from literature. There are no data close to the peak of RV curve. [Nasseri et al., 2014]

450-890 nm.

Another 62 spectra were made by spectrograph HERCULES located in University of Canterbury Mount John Observatory (UCMJO). HERCULES is a fibre-fed echelle spectrograph at 1-meter McLellan Telescope, which is a Dall-Kirkham reflector. Three spectral resolutions are possible: $R \sim 41\,000$, $R \sim 70\,000$ and $R \sim 82\,000$.

These spectra were observed between RJD 59 661 and RJD 59 689 (March and April 2022) and they cover a wavelength interval 390-750 nm.

At first, only the above mentioned spectra were analysed. In later stages of this work, 49 more high resolution echelle spectra ($R \sim 50\,000$) were used. These spectra cover time interval from May 1999 to October 2013 and their wavelength range is 362-853 nm. 26 of them were taken at ESO spectrograph FEROS during RJDs 51 327-56 099. 2 of the spectra were obtained from ESO 1.52 m telescope, the rest comes from MPG/ESO 2.2m telescope located at ESO's La Silla Observatory.

23 spectra originate from BESO spectrograph attached to the 1.5m Hexapod-Telescope. They were taken between RJD 54 913 and RJD 56 586. BESO is a clone of the spectrograph FEROS and is located at the Observatorio Cerro Armazones (OCA) in Chile.

3.2 Methods and programs

3.2.1 ReSpefo

All the CHIRON spectra I obtained were already reduced to the form of 1-D spectra. I further processed the spectra in program reSpefo (version 2) written by A. Harmanec[1].

ReSpefo is a newer version of program Spefo by J. Horn ("Simple, Yet Powerful Program for One-Dimensional Spectra Analysis"), which was written in Turbo Pascal. ReSpefo is written in Java and has several functions meant for 1-D spectra analysis. For example, its user can normalise spectra, compare them, measure radial velocities and equivalent widths of spectral lines.

All the spectra had to be normalised using the function Rectify. First, a polynomial blaze function is used to estimate the height of each echelle order, as is shown in Figure 3.2. The program then makes an estimation of the continuum level of each echelle order based on the blaze function. Then, one can choose individual orders of the spectrum and further manually adjust their continuum level.
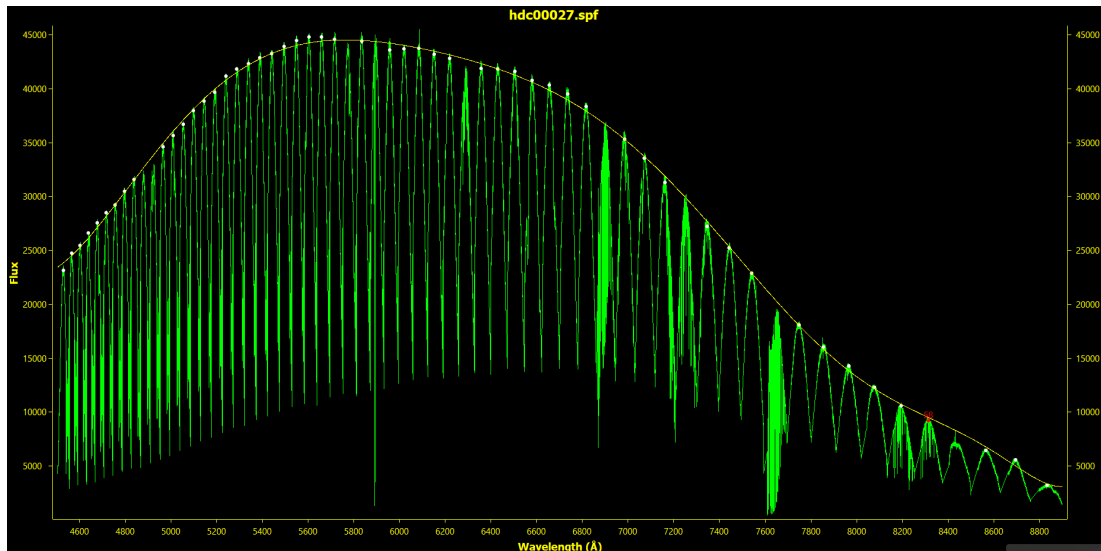
Figure 3.2: An example of a CHIRON spectrum with its blaze function in reSpefo.

In each CHIRON spectrum I chose and rectified 11 consequent orders in wavelength interval from 4615 Åto 5085 Åand one order in which the He I (6678 Å) is located. An example of normalized part of a CHIRON spectrum is in Figure 3.3. All the other echelle orders were rectified automatically using the continuum level estimation from the blaze function.

The intensity at the edge of the echelle orders is lower than in their center. Because of that the signal to noise ratio at the edge is roughly 10 times lower than in the center. Consequently the rectified spectra are more noisy in places where the echelle orders overlap (see Figure 3.3).

---

[1]The newest version of this program together with its user manual is available on website
https://astro.troja.mff.cuni.cz/projects/respefo/.

After the spectra were normalised, I measured positions of telluric lines using function Measure RV. In ReSpefo, radial velocity measurement are done via comparison of direct and horizontally flipped spectral line. The flipped line can be moved until it aligns with the direct line. From this position of lines, the program determines the radial velocity.

Heliocentric wavelengths of the spectra were slightly adjusted according to the measurements the telluric lines.

All the HERCULES spectra that I obtained were already normalised. I measured the telluric lines for these spectra as well and used them to a fine correction of the zero point of the wavelength scale.

Function Clear allows the user to clean the spectrum from cosmic ray hits and excessive noise. This was also done for both CHIRON and HERCULES spectra.
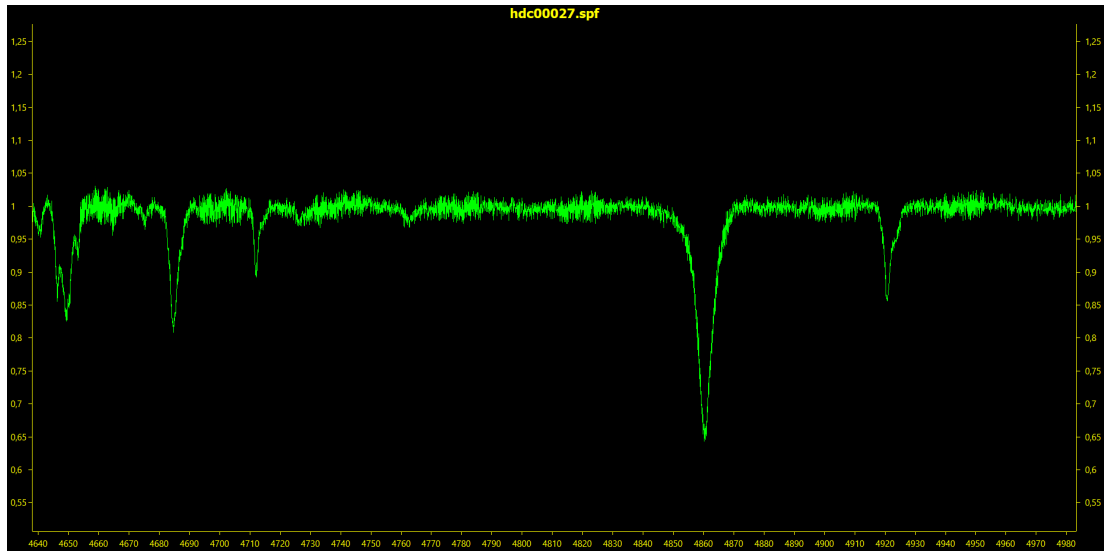
Figure 3.3: Rectified part of the same spectrum as in the previous figure.

3.2.2 KOREL

KOREL is a program that disentangles spectra of spectroscopically variable stellar systems. It can decompose the observed spectrum into spectra of individual components, measure radial velocities and determine orbital elements and other parameters of the system. All these quantities are calculated together as the best fit of the observed spectra (Hadrava [1995],Hadrava [2004b]).

In order to disentangle the observed spectra, Korel uses Fourier transform. Let us suppose that the spectrum of each star in the system $I_j(t)$ is constant in time except for being Doppler shifted because of its instantaneous radial velocity v_j. The observed spectrum of a stellar system at a time t can be then expressed as a sum of convolutions with correspondingly shifted Dirac delta distributions

$$I(x,t) = I_1(x) * \delta[x - v_1(t)] + I_2(x) * \delta[x - v_2(t)] + ... \qquad (3.1)$$

With multiple spectra obtained at different times, this becomes a huge set of linear equations. If the radial velocities $v_j(t)$ are known, the equations can be

solved for the spectra I_j. The Fourier transform of this equation is

$$\tilde{I}(y,t) = \tilde{I}_1(y)\exp\left(iyv_1(t)\right) + \tilde{I}_2(y)\exp\left(iyv_1(t)\right) + ... \tag{3.2}$$

The Fourier transform splits the original large set of linear equations into many smaller systems with dimension equal to the number of stars in the observed system. To obtain the spectra of the components, KOREL uses the simplex method to find the lowest sum of integrated squares of differences between the observed and model spectra. The search for the lowest sum is done with respect to both the orbital parameters of the system (which constrain the possible values of radial velocities) and the spectra of its stars.

Simplex is a set of $m+1$ points in the parameter space $\mathbb{R}^m$, where m is the number of parameters of the system. The sum of squares is calculated for each point of the simplex. The point with the highest sum of squares is then replaced with a different point constructed by one of the following operations applied on the original simplex: reflection, expansion, contraction or multiple contraction.

A comparison of the method used in KOREL with the classical methods of analysing spectra of multiple stellar systems is shown in Figure 3.4

KOREL is able to solve orbits of stellar systems with up to 5 components. The hierarchical structure of such system is shown in Figure 3.5. The fifth component can be also used to disentangle the telluric lines if they are present in the spectra.

3.2.3   Preparing the data for KOREL

KOREL expects the input data file in a specific format. I used programs SN2, SNVAHY and HEC35D written by P. Harmanec to convert all the spectra into an input data file for KOREL. All these programs together with a user manual can be found on website `https://astro.troja.mff.cuni.cz/ftp/hec/HEC35/`.

First I converted all the rectified and cleaned spectra into ASCII files using ReSpefo. Then I created a file called *prekor.lst* containing names of all the spectra files and their times (in RJD) in a specific format.

Program SN2 requires list of spectra in the form of file *prekor.lst*. It calculates signal to noise ratio (S/N) in a chosen region of continuum of all the spectra written in the file.

Program SNVAHY then calculates weights of each spectrum proportional to the square of its S/N ratio. It creates a new file *prekor.lst* and there it writes names of all the spectral files together with their weights and RJDs. The weight equal to 1 corresponds to the mean value of $(S/N)^2$ of all the spectra. This program also discards all spectra with the S/N ratio lower than a certain treshold. In this work the minimum acceptable value of signal to noise ratio was set to 50. Only 3 spectra (1 CHIRON and 2 HERCULES) had S/N lower than 50, all the others were further used in another program to create a final datafile for KOREL.

At last, program HEC35D produces input file *korel.dat* for KOREL while taking into account the weights of spectra in the file *prekor.lst* created by the program SNVAHY.

To disentangle the spectra, I used a version of the program KOREL that is currently available as a Virtual Observatory (VO-KOREL) on website `https://stelweb.asu.cas.cz/vo-korel/` [Škoda and Hadrava, 2010][Škoda et al., 2012].
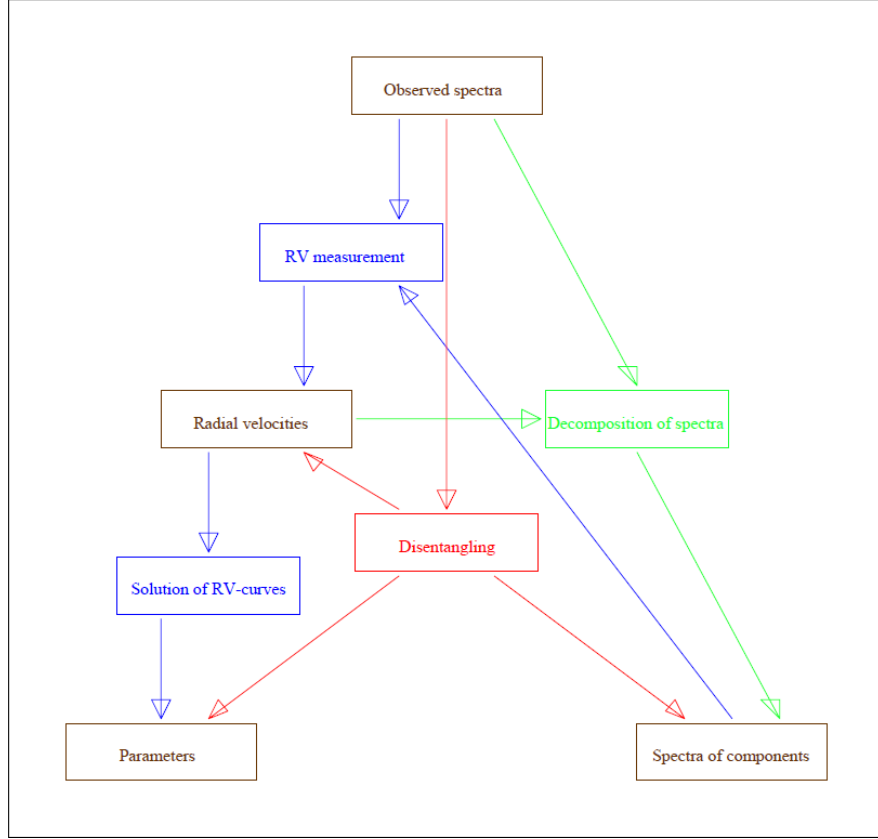
Figure 3.4: Comparison of classical methods of processing multiple star spectra with disentangling of the spectra. Normally the system's parameters can be determined from radial velocity curves. In order to measure radial velocities, it is necessary to distinguish spectral lines of individual stars. In KOREL, the spectra of individual components, radial velocities and all the orbital parameters of the system are determined together as the best fit of the observed spectra. Image credit: [Hadrava, 2009]

3.2.4 FOTEL

Another program I used for the data analysis is called FOTEL [Hadrava, 2004a]. It is a FORTRAN program that calculates orbital elements of a binary or a triple star. FOTEL can find separate solutions of light curves and radial velocity curves or it can solve them simultaneously. It is also possible to calculate linear changes of the orbital elements in time. The program uses three-axial approximation to find solutions of light curves.

The orbital solution is the minimum of the sum $\Sigma(O - C)^2$, where O are observed and C are model values of variables. In order to find the minimum of the sum of squares, FOTEL uses the simplex method described in subsection 3.2.2.

Since HD 152246 is not an eclipsing system, I only used FOTEL to find a solution of RV curves.
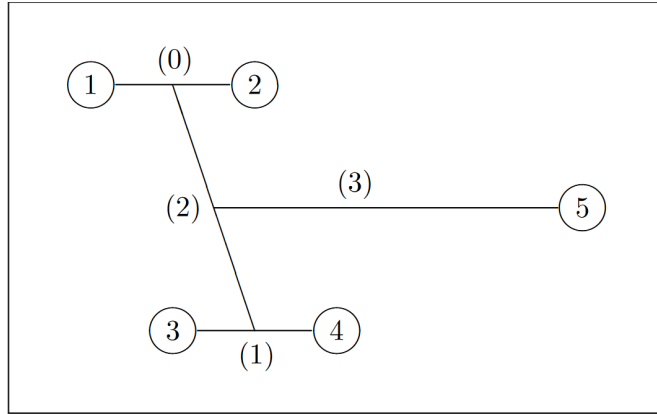
Figure 3.5: The structure of a hierarchical stellar system that can be solved by KOREL. The numbers in circles denote stars and the numbers in parentheses denote their orbits as they are used in KOREL. The same denotation of stars is used throughout the whole thesis. Image credit: Hadrava [2004b]

3.3   Results

I used KOREL on 7 short spectral segments from the CHIRON and HER-CULES spectra containing following spectral lines:

- He II 4685.682 Å,

- He I 4713.203 Å,

- H-beta 4861.332 Å,

- He I 4921.931 Å,

- He I 5015.678 Å,

- He I 6678.151 Å.

The seventh segment contained several blended lines:

- C III 4647.418 Å,

- O II 4649.143 Å,

- C III 4650.246 Å,

- O II 4650.847 Å,

- C III 4651.025 Å,

- C III 4651.473 Å,

- C III 4652.048 Å,

- Si IV 4654.312 Å.

Finally I used KOREL on a longer section in the blue part of the spectra with the wavelength interval from 4635 Å to 5050 Å.

Each one of these 8 spectral regions was converted into KOREL input file using the process described in subsection 3.2.3.

Besides the input data file KOREL also requires a parameter file. This file includes code that controls the run of the program as well as specifies initial estimates of the system's parameters. The final values of parameters from Nasseri et al. [2014] were used as initial estimates in my KOREL runs (see Table 3.3). I used the values of both orbital periods determined by Nasseri et al. [2014] ($P_{\mathrm{in}} = 6.004865$ d, $P_{\mathrm{out}} = 470.69$ d.) and I kept them fixed during my KOREL runs.

I did several trial KOREL runs to fins a solution with the lowest sum of residuals. Each time I adjusted the element estimates in the parameter file according to the previous solution. The final solutions for all of the eight spectral segments are written in Table A.2. For each of them I also calculated the mass function of the inner binary according to formula 2.16.

KOREL does not calculate errors, so I calculated mean value and standard deviation of the 8 independent solutions (Table 3.4). This way I can at least estimate uncertainties of the orbital elements.

KOREL provides radial velocity values alongside the orbital elements. Since I obtained 8 sets of RV measurements (from the 8 solutions), I calculated mean and standard deviation for each RJD. These values are summarized in Table A.1 in the attachments. Radial velocity curve is plotted in Figure 3.6.

The disentangled spectra (in the interval 4635-5050 Å) of the two O-type stars are shown in Figure 3.7. There are several lines of Helium, H-beta line and blended lines of C III, O II a Si IV. I tried to disentangle some weaker lines of the cooler star 2 as well, but with no success.
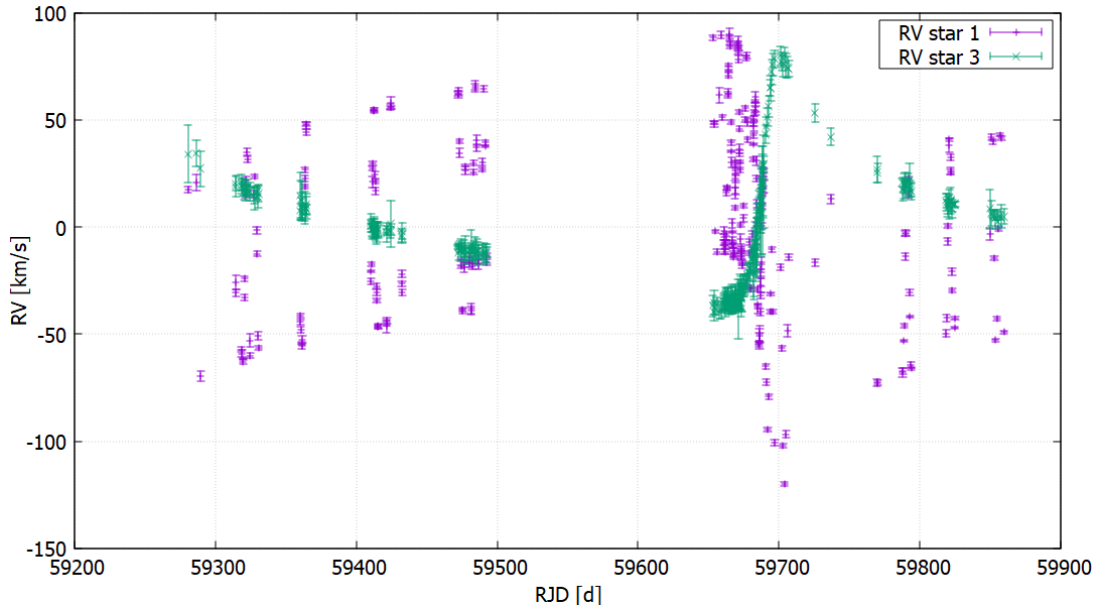
Figure 3.6: Radial velocities measured by KOREL.
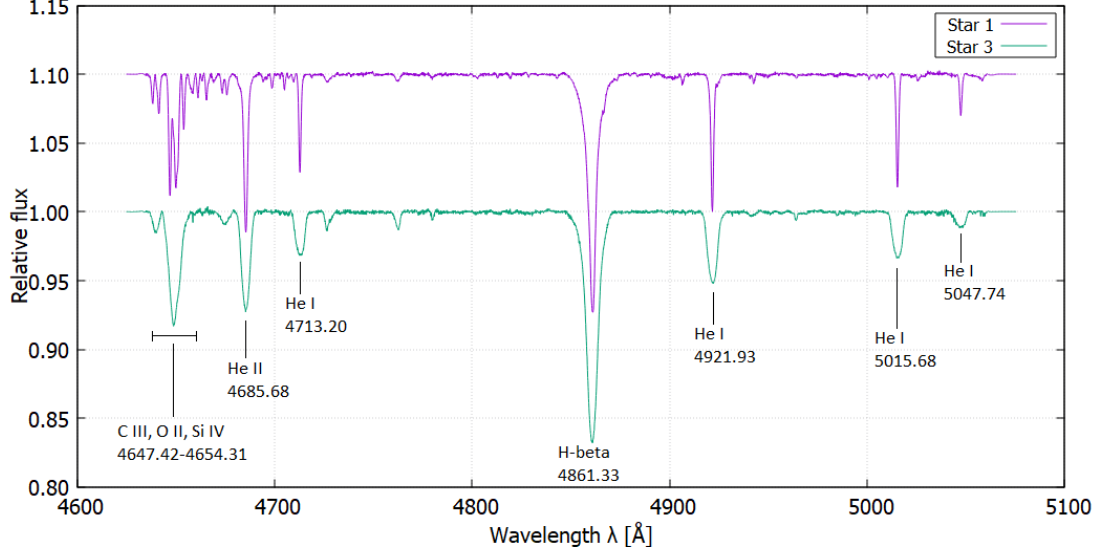
Figure 3.7: Normalised disentangled spectra, spectrum of the first star is shifted upwards by 0.1.

Table 3.4: KOREL solution for CHIRON & HERCULES spectra - mean values of orbital elements

Element	Mean value	Standard deviation
Short orbit		
T_p (RJD)	59671.3443	0.0021
e	0.0831	0.0033
ω_p (°)	37.040	0.032
K_1 (km.s^{-1})	51.10	0.31
$f(m)$ (M$_\odot$)	0.0822	0.0014
Long orbit		
T_p (RJD)	59691.54	0.23
e	0.7508	0.0024
ω_p (°)	118.95	0.63
K_{1+2} (km.s^{-1})	55.05	0.96
q	0.992	0.014
K_3 (km.s^{-1})	55.5	1.2

Comparing my results from the newer CHIRON and HERCULES spectra in Table 3.4 to the elements derived by Nasseri et al. [2014] in Table 3.3 shows large differences. The dense coverage of the periastron passage allows for a more precise determination of both eccentricity and RV semi-amplitude of the outer orbit. Namely the new eccentricity value $e \approx 0.75$ is considerable lower than the problematic $e = 0.865$.

My next step was using KOREL on the older BESO and FEROS spectra. This time I fixed the eccentricity of the outer orbit as $e = 0.75$. As initial estimates of

the elements I used the average of my results for the CHIRON and HERCULES spectra. I re-calculated the times of periastron passage so that they would be inside the time interval covered by the spectra.

My main goal was to find out whether there had been some changes in the values of orbital elements. After several trial solutions I found out that I get better results (lower values of $O - C$) when I use value $K_1 = 34.6 \, \mathrm{km \, s^{-1}}$ as the initial estimate for the RV semi-amplitude of star 1 on the inner orbit. It is the value derived in the article Nasseri et al. [2014]. The RV semi-amplitude K_1 is clearly changing in time.

I calculated mean values and standard deviations of all elements (as I did for the CHIRON and HERCULES solutions), they are written in Table 3.5. Comparing the results in Tables 3.4 and 3.5 shows that the semi-amplitude of RV of the inner orbit (K_1) changes considerably in time.

The BESO spectra are very noisy in the blue part of the spectrum on which I focused. The weights assigned to BESO spectra were significantly lower than the weights of FEROS spectra, which means that the FEROS spectra had much higher impact on the KOREL solution. The BESO spectra have a much better signal to noise ratio around the spectral line He I 6678. For this line, the BESO and FEROS had similar impact on the results from KOREL.

Later I only used a combination of the older FEROS spectra and the newer CHIRON and HERCULES spectra. In this case I let KOREL compute the orbital solution while assuming a non-zero value of the time derivative of the RV semi-amplitude K_1. KOREL is only able to compute linear changes of the orbital parameters in time. The change of K_1 is most likely non-linear. To take this effect into account properly, it is necessary to use a different approach.

Table 3.5: KOREL solution for BESO & FEROS spectra - mean values of orbital elements

Element	Mean value	Standard deviation
Short orbit		
T_p (RJD)	54285.271	0.085
e	0.086	0.040
ω_p (°)	36.7	3.0
K_1 (km.s^{-1})	35.69	0.72
$\dot{K}_1$ (km.s^{-1}.100yr^{-1})	0.00301	0.00070
$f(m)$ (M$_\odot$)	0.0279	0.0016
Long orbit		
T_p (RJD)	54985.1	1.4
ω_p (°)	114.9	4.6
K_{1+2} (km.s^{-1})	52.2	3.7
q	0.988	0.006
K_3 (km.s^{-1})	52.8	3.6

Table 3.6: KOREL solution for FEROS, CHIRON & HERCULES spectra - mean values of orbital elements

Element	Mean value	Standard deviation
Short orbit		
T_p (RJD)	59671.408	0.043
e	0.091	0.005
ω_p (°)	38.05	1.22
K_1 (km.s^{-1})	51.8	1.5
$\dot{K}_1$ (km.s^{-1}.100yr^{-1})	0.0024	0.0003
$f(m)$ (M$_\odot$)		
Long orbit		
T_p (RJD)	59691.92	0.31
ω_p (°)	121.0	1.8
K_{1+2} (km.s^{-1})	52.94	1.21
q	0.97	0.02
K_3 (km.s^{-1})	54.5	1.9

Next I used the program FOTEL as another independent way of determining the orbital parameters. This way I could also verify the results obtained from KOREL. FOTEL calculates the orbital elements directly from radial velocity curve, so I measured RVs in ReSpefo. I measured RVs on the following three lines:

- He I, 4923.931 Å,

- He I, 5875.732 Å,

- He I, 6678.151 Å.

I calculated the average values of RVs measured on the three lines and used them as input for FOTEL. These average RVs are plotted in graph in Figure 3.8. The errors are calculated as standard deviations of the measured values.

A comparison of radial velocities calculated by KOREL and measured in ReSpefo is in Figure 3.9. The trend of both sets of RVs is clearly the same, but the radial velocities measured in ReSpefo are systematically lower than those obtained from KOREL. Nevertheless, the KOREL RVs are still within the uncertainty intervals of ReSpefo RVs (since they are quite large, up to $30\,\mathrm{km\,s^{-1}}$).
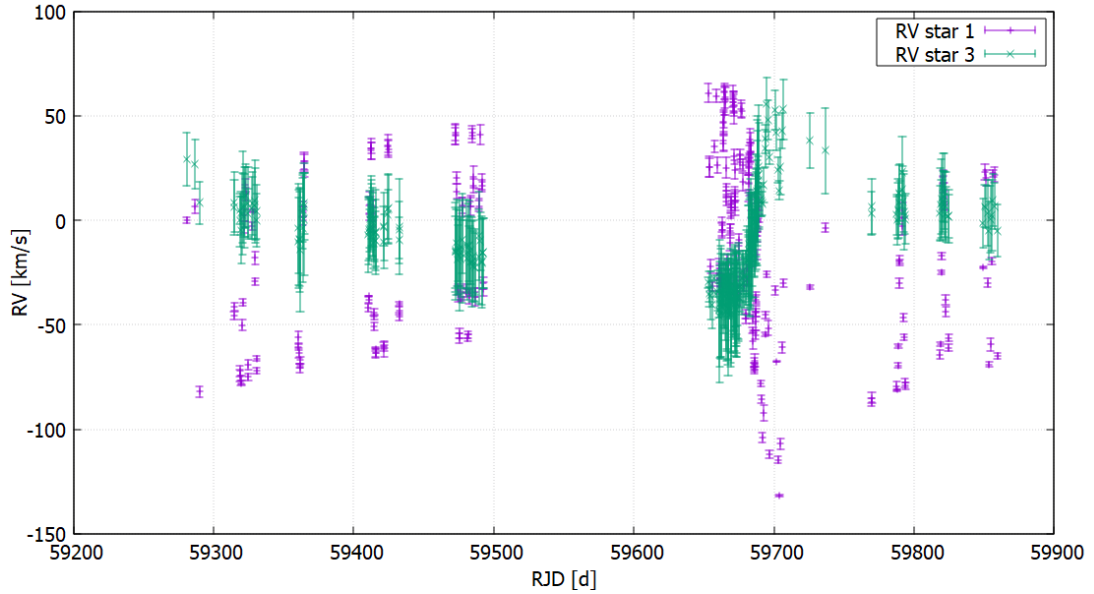
Figure 3.8: Radial velocities measured in ReSpefo.
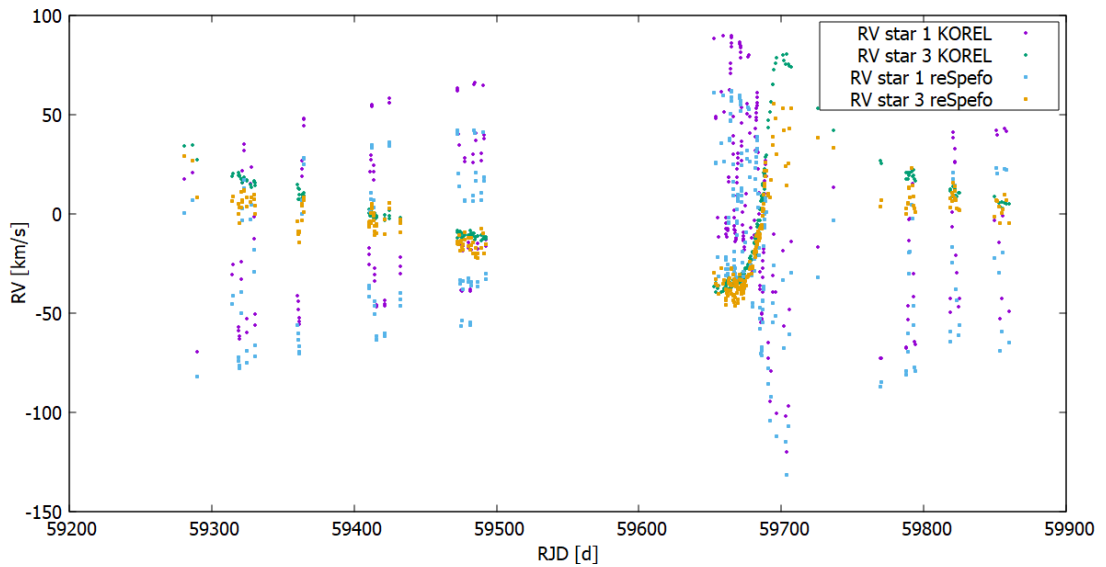
Figure 3.9: Comparison of measured radial velocities.

Measuring of radial velocities in ReSpefo is very subjective, because the positions of spectral lines are estimated by the user. The spectral lines of star 1 are narrower and deeper than the lines of star 3 and they are blended together. When measuring RVs of star 1, I estimated the position of the core of its spectral lines. For spectral lines of star 3, I measured the position of their wings. As an example of this process, the profile of blended spectral lines He I 4923 is shown in Figure 3.10. The core of the primary star's line is clearly visible and the radial velocity of this star can be measured easily. The core of third star's line is not visible, so it is necessary to measure the position of its wings. The sketches in Figures 3.11 and 3.12 show the blended profile for a narrower and a wider profile

of the third star. On the first sight, both cases look similar. I measured the position of the wings of the whole blended profile, but the lines of the star 3 are most likely somewhat narrower. This way of measuring caused a systematic error in the values of radial velocity. However, the measurements are still good enough for their purpose - to verify the results obtained from KOREL.
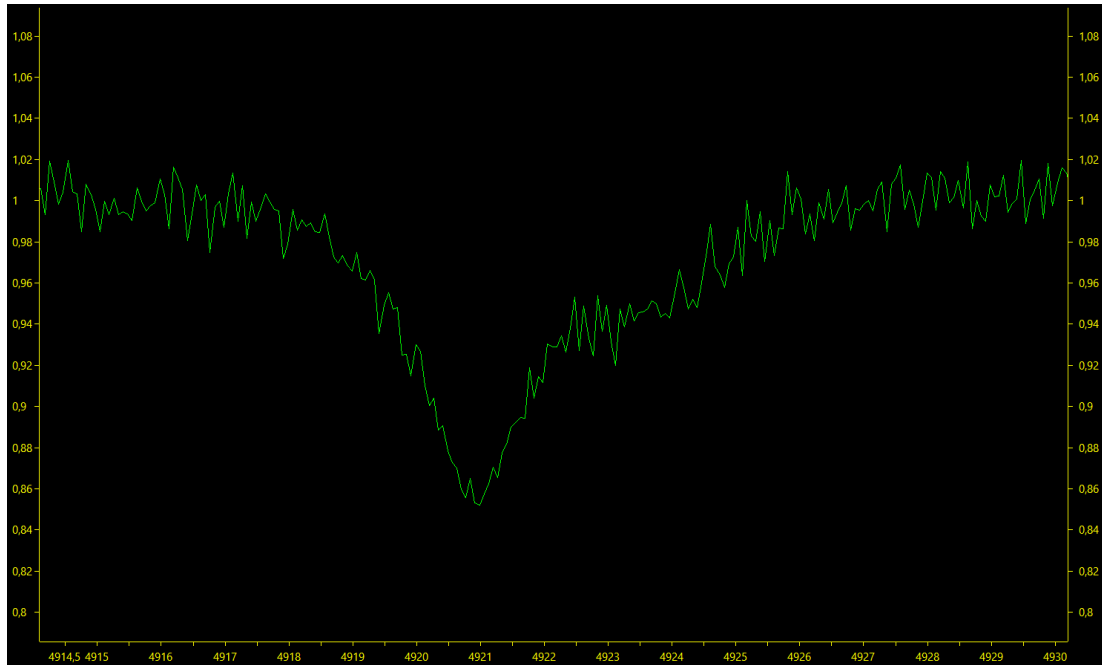
Figure 3.10: The profile of observed spectral line He I 4923.
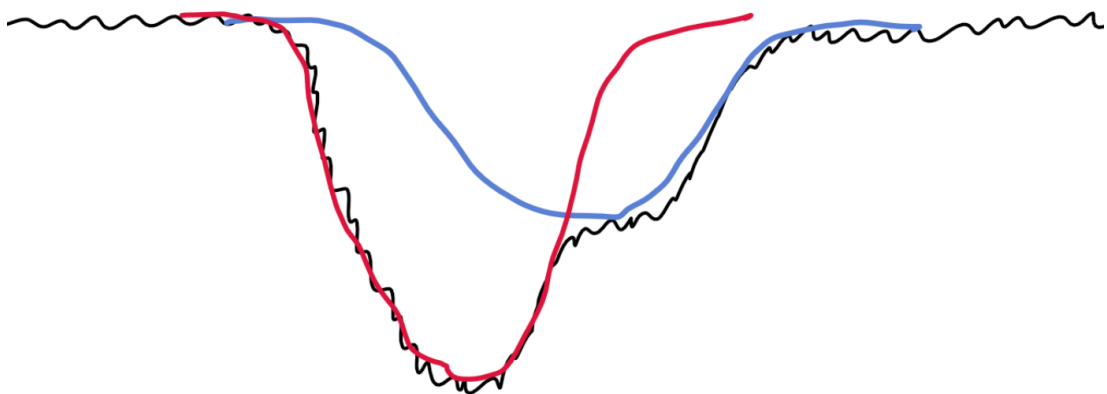
Figure 3.11: The profile of blended lines with a narrower line of the third star.
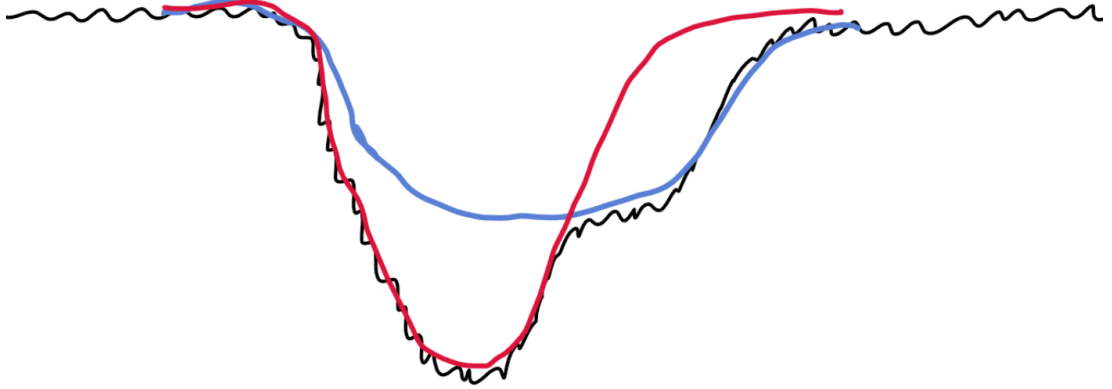
Figure 3.12: The profile of blended lines with a wider line of the third star. This is the way I measured RVs in ReSpefo.

I used FOTEL on 4 sets of RVs. I measured RVs in ReSpefo on three convenient spectral lines: He I 5876, He I 6678 a He I 4923. For each RJD, I calculated the average value of radial velocity v, its standard deviation σ_{v} and then the average of all standard deviations σ (see Table A.1). I calculated the weight of measurements as follows

$$w_{\mathrm{v}} = \frac{\sigma^2}{\sigma_{\mathrm{v}}^2} \tag{3.3}$$

This way I normalised the weights, so that measurements with $\sigma_{\mathrm{v}} = \sigma$ have unit weight $w = 1$.

Using program VOLBA written by P. Harmanec, I created an input file for FOTEL. I also had 7 RVs for each RJD measured by KOREL on which I applied the same procedure. The FOTEL solution for these two sets of RVs is in Table 3.7. Unlike KOREL, FOTEL calculates also errors of the orbital parameters. The errors I estimated from the KOREL solution (see Table 3.4) are 1-3 orders higher and more realistic than the errors calculated by FOTEL.

In the output file of FOTEL there is also included a table with radial velocities and their corresponding orbital phases as well as residuals after the subtraction of the motion in the inner and outer orbit, respectively. I used this to create phase diagrams for both the inner (Figures 3.13, 3.14) and outer orbit (Figures 3.15, 3.16).

The RV semi-amplitudes of the 470-day orbit derived by FOTEL from RVs I measured in ReSpefo are only about 37 km.s^{-1}. This is considerably lower than the semi-amplitudes derived from KOREL velocities, which is about 57 km.s^{-1}. (see Table 3.7). It can be clearly seen in the phase diagrams as well (see Figures 3.15 and 3.16). This is caused by the way I measured RVs in ReSpefo

and their consequent systematic errors. All the other orbital elements are in good agreement.

The position of the deeper and narrower lines of star 1 can be measured more easily. Due to that, the systematic errors of its radial velocities are small. Consequently, the elements of the 6-day orbit derived by FOTEL from ReSpefo RVs are in good agreement with the ones derived from KOREL velocities (see Table 3.7 and phase diagrams 3.13 and 3.14).

Later I created two new sets of RVs - I united the RVs from years 2021-2022 measured on CHIRON and HERCULES spectra with older values of RV from years 1999-2013 taken from literature. In this case I let FOTEL calculate also the change of RV semi-amplitude $\dot{K}_1$. The results are summed up in Table 3.8.

Finally I plotted a phase diagram of the 6-day orbit with both the newer (2021-2022) and older (1999-2013) values of RVs (see Figure 3.17). I plotted each of the two sets with different colour to emphasize the change in RV semi-amplitude K_1. A phase shift between the two data sets is also visible in the figure. This indicates that the fixed 6-day period I used in all my calculations could be determined more precisely. I kept the periods fixed to be able to calculate other orbital parameters and the change of K_1.

Values of the RV semi-amplitudes corresponding to the outer orbit (K_3 and K_{1+2}) in Tables 3.4 and 3.5 suggest that K_3 and K_{1+2} are changing in time as well. Since the change of K_3 and K_{1+2} is comparable to their respective uncertainties, it is necessary to obtain more spectroscopic observations of the systems to confirm it. It would be also useful for determining a more precise values of both the 6-day and the 470-day orbital periods. The change of radial velocity semi-amplitude implies a change of inclination of the orbit. It seems that the inclinations of both the inner and outer orbit are changing in time.

Table 3.7: Orbital solutions for radial velocities measured on CHIRON and HER-CULES spectra. The orbital elements were calculated in program FOTEL.

RV measured in	ReSpefo	KOREL
Short orbit		
T_p (RJD)	59671.40 ± 0.14	59671.32 ± 0.03
e	0.080 ± 0.009	0.082 ± 0.002
ω_p (°)	40.1 ± 8.7	35.9 ± 1.5
K_1 (km.s^{-1})	49.1 ± 1.2	51.1 ± 0.1
Long orbit		
T_p (RJD)	59691.43 ± 0.01	59691.433 ± 0.002
e	0.7376 ± 0.0002	0.75162 ± 0.00004
ω_p (°)	119.69 ± 0.04	118.749 ± 0.004
K_{1+2}/K_1	1.01 ± 0.03	1.066 ± 0.004
K_3 (km.s^{-1})	37.15 ± 0.02	57.541 ± 0.006

Table 3.8: Orbital solutions for both radial velocities measured on CHIRON and HERCULES spectra and older radial velocities from literature. The orbital elements were calculated in program FOTEL.

RV measured in	ReSpefo	KOREL
Short orbit		
T_p (RJD)	59671.41 ± 0.16	59671.2 ± 0.2
e	0.080 ± 0.010	0.082 ± 0.012
ω_p (°)	40.1 ± 9.7	28.3 ± 9.2
K_1 (km.s^{-1})	49.0 ± 1.4	50.9 ± 1.4
$\dot{K}_1$ (km.s^{-1}.100yr^{-1})	74 ± 10	88 ± 12
Long orbit		
T_p (RJD)	59691.68 ± 0.01	59691.60 ± 0.01
e	0.7316 ± 0.0002	0.7503 ± 0.0003
ω_p (°)	119.68 ± 0.04	118.05 ± 0.03
K_{1+2}/K_1	1.02 ± 0.04	1.11 ± 0.03
K_3 (km.s^{-1})	39.74 ± 0.02	54.15 ± 0.03
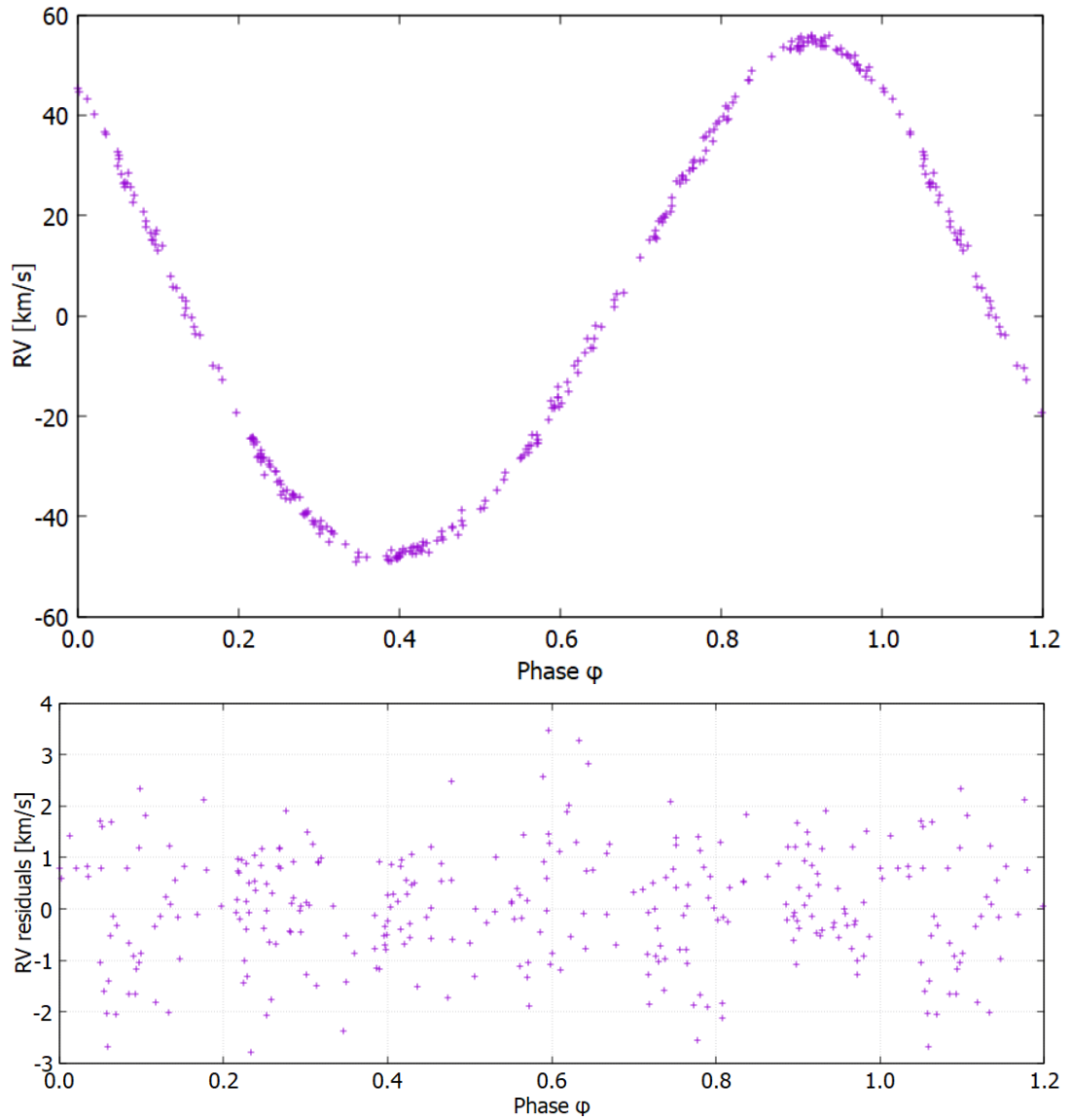
Figure 3.13: Top figure: Phase diagram for radial velocities of component 1 on the short orbit. Gamma velocity and changes in RV due to motion on the long orbit are already subtracted. Graph uses RV values measured in KOREL. Bottom figure: RV residuals.
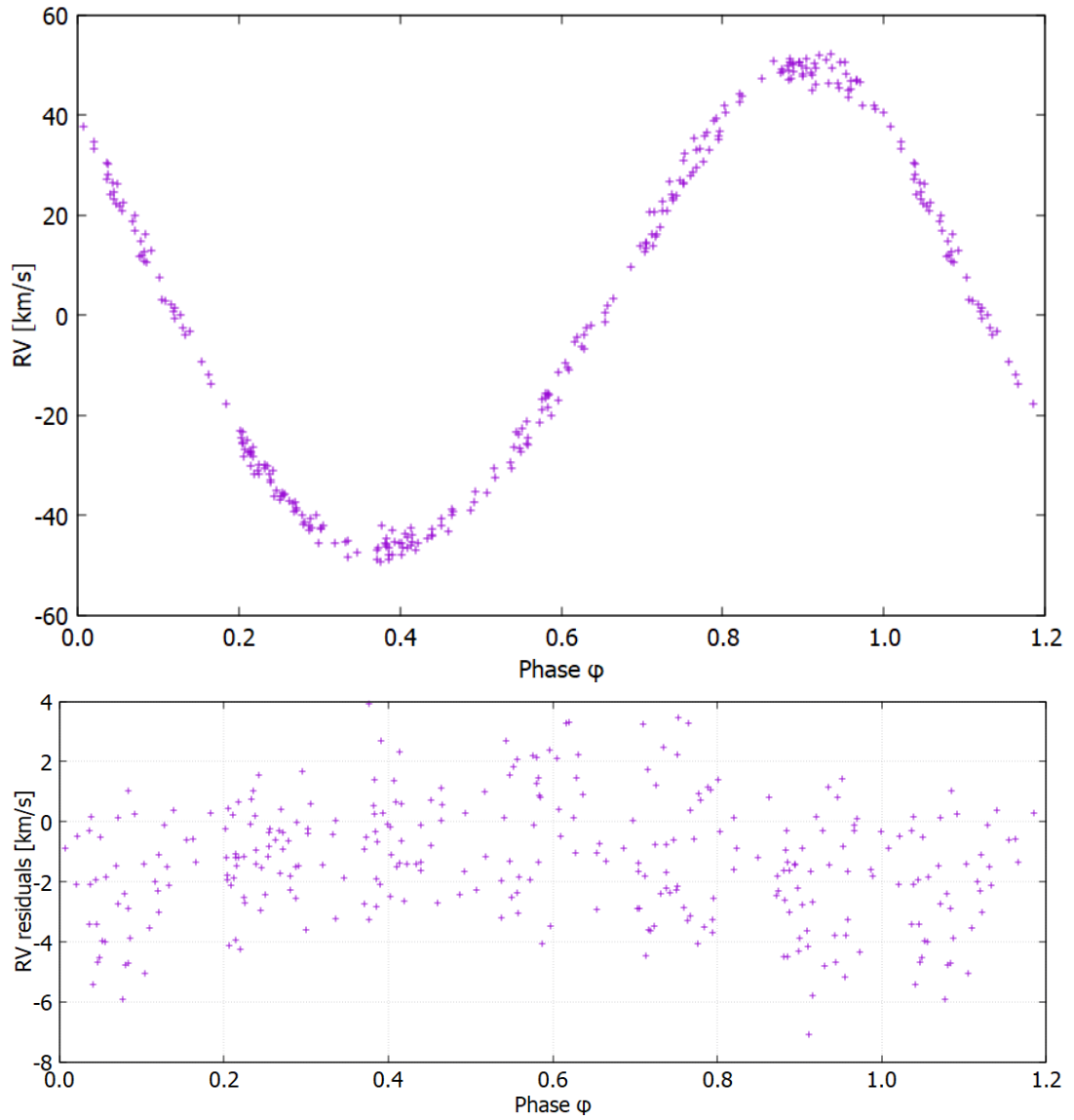
Figure 3.14: Top figure: Phase diagram for radial velocities of component 1 on the short orbit. Gamma velocity and changes in RV due to motion on the long orbit are already subtracted. Graph uses RV values measured in ReSpefo. Bottom figure: RV residuals.
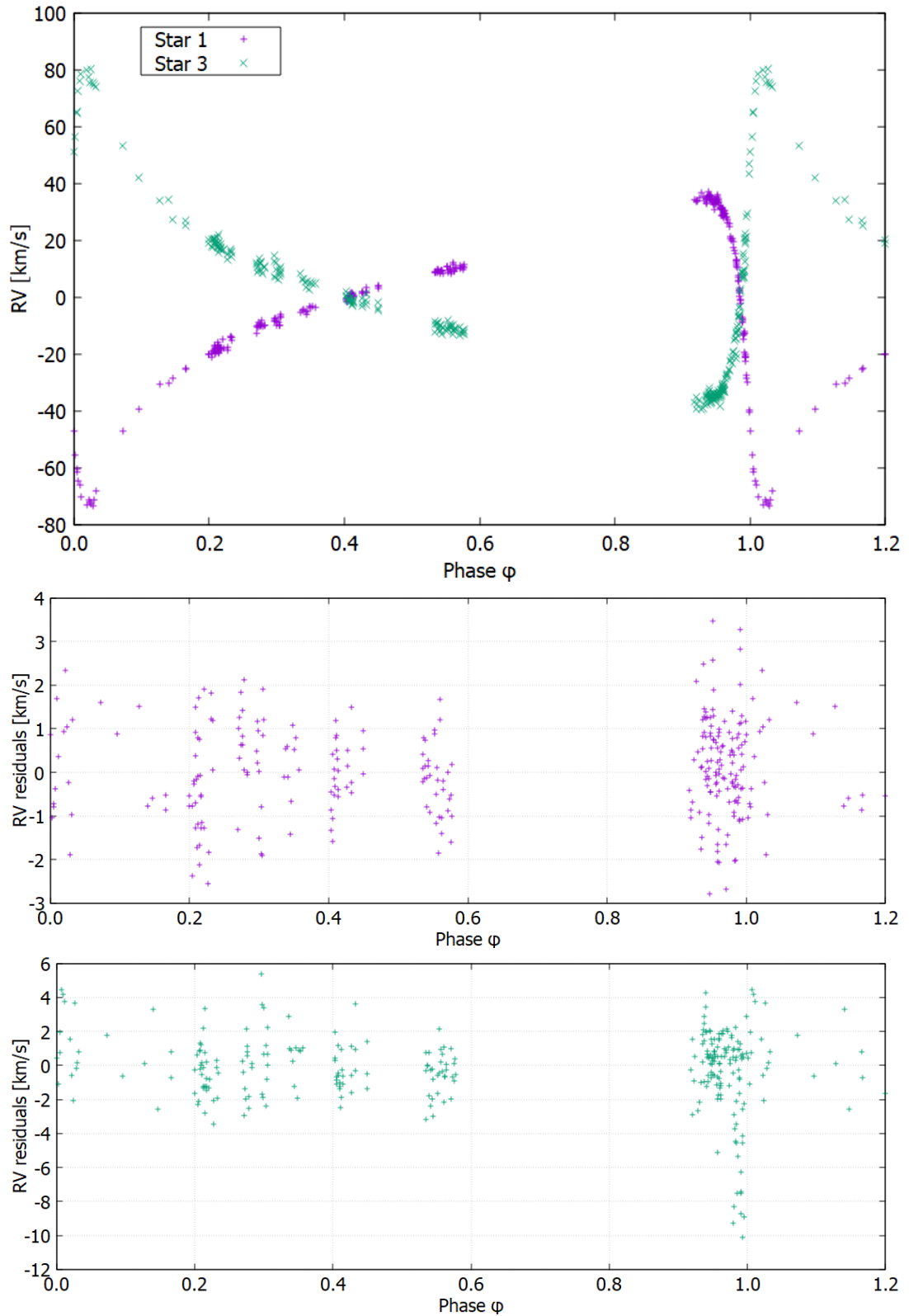
Figure 3.15: Top figure: Phase diagram for radial velocities of both components 1 and 3 on the long orbit. Gamma velocity is already subtracted. RVs of star 1 are also corrected for motion on the short orbit. Graph uses RV values measured in KOREL. Middle figure: RV residuals for star 1. Bottom figure: RV residuals for star 3.
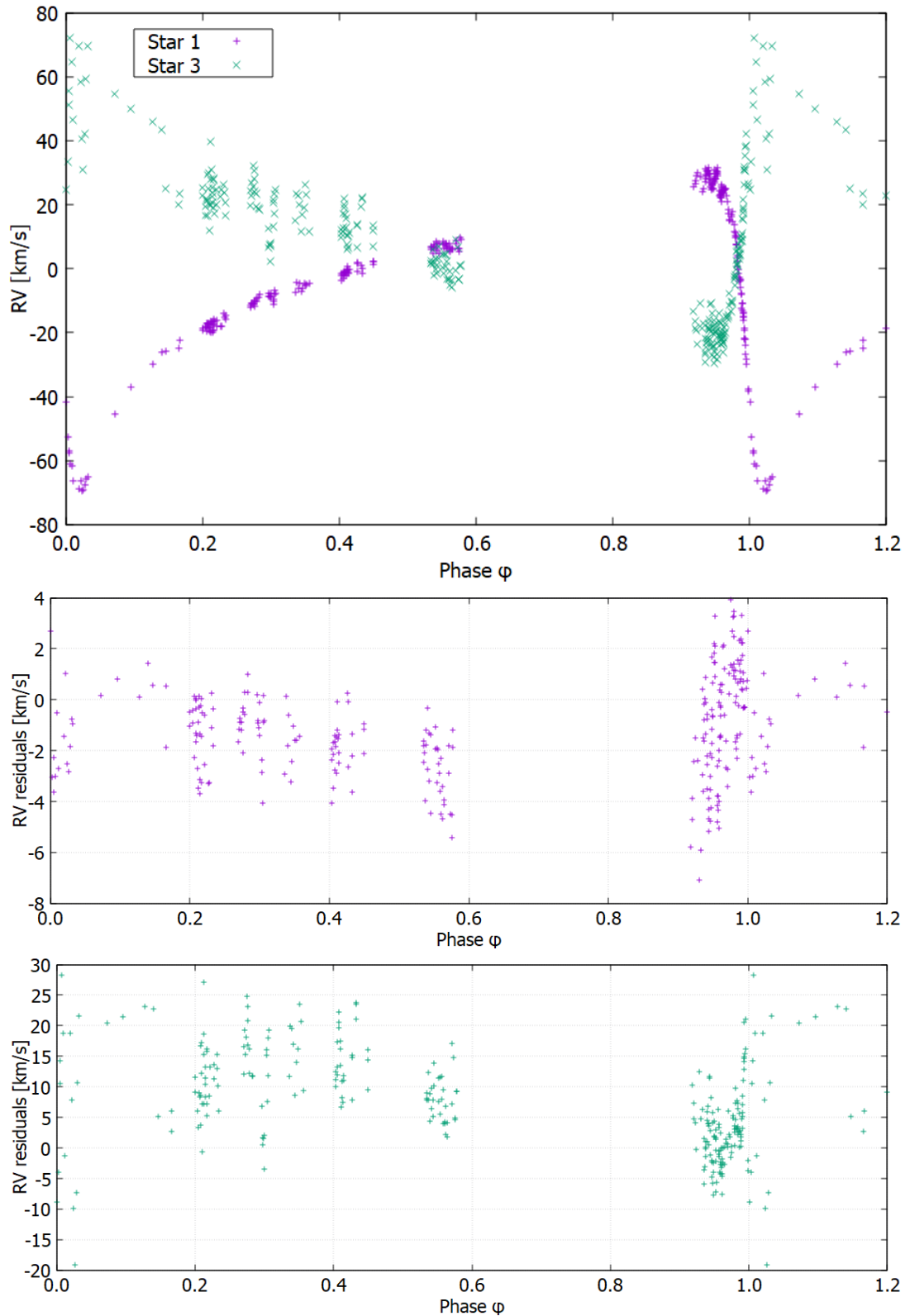
Figure 3.16: Top figure: Phase diagram for radial velocities of both components 1 and 3 on the long orbit. Gamma velocity is already subtracted. RVs of star 1 are also corrected for motion on the short orbit. Graph uses RV values measured in ReSpefo. Middle figure: RV residuals for star 1. Bottom figure: RV residuals for star 3.
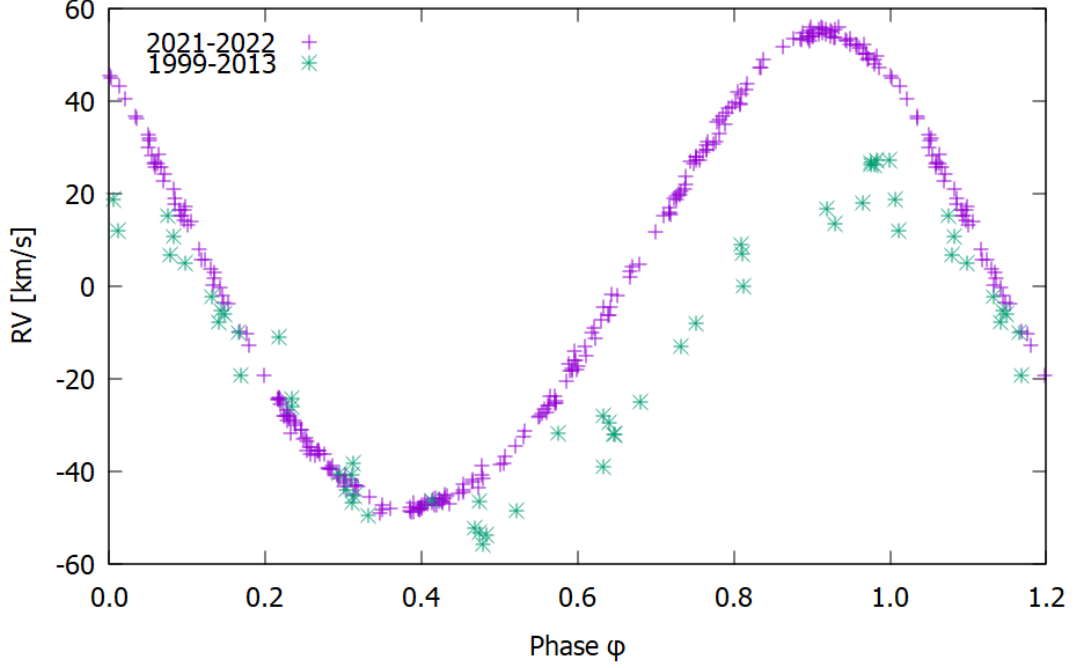
Figure 3.17: Comparison of phase diagrams for radial velocities of star 1 on the short orbit. The increase of semi-amplitude of radial velocity K_1 is quite obvious.

3.3.1 Astrometric orbital solution

The tertiary star is so distant from the close pair of primary and secondary stars that it can be interferometrically resolved. Interferometric observations can be used to find astrometric solution of the orbit.

The relative position of tertiary star with respect to primary star on the plane of the sky can be described by Cartesian coordinates x and y. The positive x direction is along North and the positive direction of y is along East. The coordinates (x, y) at a time t are

$$x = \delta_{\text{North}} = A(\cos E - e) + F\sqrt{1 - e^2}\sin E \tag{3.4}$$

$$y = \delta_{\text{East}} = B(\cos E - e) + G\sqrt{1 - e^2}\sin E \tag{3.5}$$

where $E(t)$ is the eccentric anomaly given by the Kepler's equation 2.9, e is eccentricity and A, B, F and G are Thiele-Innes constants.

The Thiele-Innes constants are defined in terms of the following orbital elements: longitude of periastron ω, longitude of the ascending node Ω, angular size of semi-major axis α and inclination i.

$$A = \alpha(\cos\Omega\cos\omega - \sin\Omega\sin\omega\cos i) \tag{3.6}$$

$$B = \alpha(\sin\Omega\cos\omega + \cos\Omega\sin\omega\cos i) \tag{3.7}$$

$$F = \alpha(-\cos\Omega\sin\omega - \sin\Omega\cos\omega\cos i) \tag{3.8}$$

$$G = \alpha(-\sin\Omega\sin\omega + \cos\Omega\cos\omega\cos i) \tag{3.9}$$

The inverse transformation is

$$\tan(\omega + \Omega) = \frac{B - F}{A + G} \tag{3.10}$$

$$\tan(\omega - \Omega) = \frac{-B - F}{A - G} \tag{3.11}$$

$$\alpha(1 + \cos i) = \frac{A + G}{\cos(\omega + \Omega)} = \frac{B - F}{\sin(\omega + \Omega)} \tag{3.12}$$

$$\alpha(1 - \cos i) = \frac{A - G}{\cos(\omega - \Omega)} = \frac{-B - F}{\sin(\omega - \Omega)} \tag{3.13}$$

The eccentricity $e = 0.75$, orbital period $P_{\text{out}} = 470.69\,\text{d}$ a time of periastron passage $T_{\text{p}} = 59691.5$ are already known from the analysis of spectroscopic data. Now they can be used to determine the astrometric orbit of the system.

I used 5 newly processed interferometric measurements from the Optical inter- ferometry DataBase [2].The observations were made by the PIONIER four beam combiner [Le Bouquin et al., 2011] at the four Auxiliary Telescopes of the ESO Very Large Telescope Interferometer (VLTI). A summary of these measurements is in Table 3.9. The data reduction was done by A. Oplištilová.

Three of the measurements have been already used by Nasseri et al. [2014], but their values of coordinates (x, y) are slightly different from the ones I used. However the difference in error estimation is quite large. The uncertainties of their data points were more than 10 times higher than the uncertainties of my data. The new, lower values should be a better estimate.

Table 3.9: Interferometric measurements of HD 152246

RJD	Date	$\delta_{\text{North}}(\text{mas})$	$\delta_{\text{East}}(\text{mas})$	$M(°)$	$E(°)$
56712.34	24.2.2014	-2.0432 ± 0.0072	-2.6364 ± 0.0089	241.44	216.11
56751.28	4.4.2014	-2.2343 ± 0.0025	-2.2165 ± 0.0048	271.22	235.71
56785.40	8.5.2014	-2.2443 ± 0.0091	-1.7325 ± 0.0095	297.32	255.68
58231.31	23.4.2018	-1.9819 ± 0.0043	-0.9457 ± 0.0036	323.20	281.02
59674.32	5.4.2022	-1.0201 ± 0.0029	0.0044 ± 0.0060	346.86	318.24

According to equation 2.7 I calculated the mean anomaly M. Then I calculaed the eccentric anomaly from the Kepler's equation 2.9. Both of these quantities are included in Table 3.9.

Lucy [2014] derived explicit least-squares formulae for the Thiele-Innes con- stants A, B, F, G and for their variances and covariances.

The weights of individual measurements x_{n}, y_{n} with uncertainties $\sigma_{\text{n}}^{\text{x}}$, $\sigma_{\text{n}}^{\text{y}}$ are

$$w_{\text{n}}^{\text{x,y}} = \frac{\sigma^2}{(\sigma_{\text{n}}^{\text{x,y}})^2} \tag{3.14}$$

where σ is the standard error of a measurement with weight equal to 1.
The following quantities are defined to simplify the calculation

$$a = \Sigma_{\text{n}} w_{\text{n}} X_{\text{n}}^2 \tag{3.15}$$

$$b = \Sigma_{\text{n}} w_{\text{n}} Y_{\text{n}}^2 \tag{3.16}$$

$$c = \Sigma_{\text{n}} w_{\text{n}} X_{\text{n}} Y_{\text{n}} \tag{3.17}$$

---

[2]The Jean-Marie Mariotti Center OiDB service is available at http://oidb.jmmc.fr .

$$r_{11} = \Sigma_{\text{n}} w_{\text{n}}^{\text{x}} x_{\text{n}} X_{\text{n}} \tag{3.18}$$

$$r_{12} = \Sigma_{\text{n}} w_{\text{n}}^{\text{x}} x_{\text{n}} Y_{\text{n}} \tag{3.19}$$

$$r_{21} = \Sigma_{\text{n}} w_{\text{n}}^{\text{y}} y_{\text{n}} X_{\text{n}} \tag{3.20}$$

$$r_{22} = \Sigma_{\text{n}} w_{\text{n}}^{\text{y}} y_{\text{n}} Y_{\text{n}} \tag{3.21}$$

where X and Y are functions of eccentric anomaly E and eccentricity e

$$X = \cos E - e \tag{3.22}$$

$$Y = \sin E \sqrt{1 - e^2} \tag{3.23}$$

I used weights w_{n}^{x} to calculate constants A and F and weights w_{n}^{y} to calculate B and G.

The final-least squares formulae for the Thiele-Innes constants are

$$A = \frac{b r_{11} - c r_{12}}{\Delta} \tag{3.24}$$

$$F = \frac{a r_{12} - c r_{11}}{\Delta} \tag{3.25}$$

$$B = \frac{b r_{21} - c r_{22}}{\Delta} \tag{3.26}$$

$$G = \frac{a r_{22} - c r_{21}}{\Delta} \tag{3.27}$$

where

$$\Delta = ab - c^2 \tag{3.28}$$

The numbers a, b and c are elements of a matrix $\mathbb{M}$

$$\mathbb{M} = \begin{pmatrix} a & c \\ c & b \end{pmatrix} \tag{3.29}$$

The standard errors of A, B, F, G are derived from the elements of its inverse, the covariance matrix $\mathbb{M}^{-1}$

$$\mathbb{M}^{-1} = \begin{pmatrix} \dfrac{b}{\Delta} & \dfrac{-c}{\Delta} \\ \dfrac{-c}{\Delta} & \dfrac{a}{\Delta} \end{pmatrix} \tag{3.30}$$

$$\sigma_{\text{A,B}}^2 = \frac{b}{\Delta} \sigma^2 \tag{3.31}$$

$$\sigma_{\text{F,G}}^2 = \frac{a}{\Delta} \sigma^2 \tag{3.32}$$

The estimates of Thiele-Innes constants computed from the data in Table 3.9 are

- $A = (0.727 \pm 0.003)\,\text{mas}$,

- $B = (1.695 \pm 0.005)\,\text{mas}$,

- $F = (2.355 \pm 0.005)\,\text{mas}$,

- $G = (-0.003 \pm 0.007)\,\text{mas}$.

The orbital elements calculated from inverse transformations 3.10, 3.11, 3.12 and 3.13 are

- $\omega = 118.9° \pm 0.5°$,

- $\Omega = 18.7° \pm 0.5°$,

- $\alpha = (2.55 \pm 0.08)\,\text{mas}$,

- $i = 127.98°^{+3.6}_{-3.3}$.

The astrometric orbit is plotted in Figure 3.18.

Next I calculated the semi-major axis, parallax and masses of the stars. Addition of equations 2.13 and 2.14 gives an equation for $a\sin i$

$$a\sin i = \frac{P_{\text{out}}}{2\pi}(K_{1+2} + K_3)\sqrt{1 - e^2} \tag{3.33}$$

All quantities on the right hand side are already known from the analysis of spectroscopic measurements. The semi-major axis is

$$a = (3.95 \pm 0.35)\,\text{au} \tag{3.34}$$

The parallax is

$$p = \frac{\alpha}{a} = (0.64 \pm 0.06)\,\text{mas} \tag{3.35}$$

This value of parallax is higher than the one from GAIA DR3 ($p_{\text{GAIA}} = (0,53 \pm 0,03)$ mas.

The masses can be calculated from the third Kepler law and the ratio of radial velocity semi-amplitudes.

$$M_1 + M_2 + M_3 = \frac{4\pi^2 a^3}{GP_{\text{out}}^2} \tag{3.36}$$

$$M_1 + M_2 + M_3 = (38.6 \pm 3.4)\,\text{M}_\odot \tag{3.37}$$

$$\frac{M_3}{M_1 + M_2} = \frac{K_{1+2}}{K_3} \tag{3.38}$$

$$M_1 + M_2 = (19.4 \pm 1.8)\,\text{M}_\odot \tag{3.39}$$

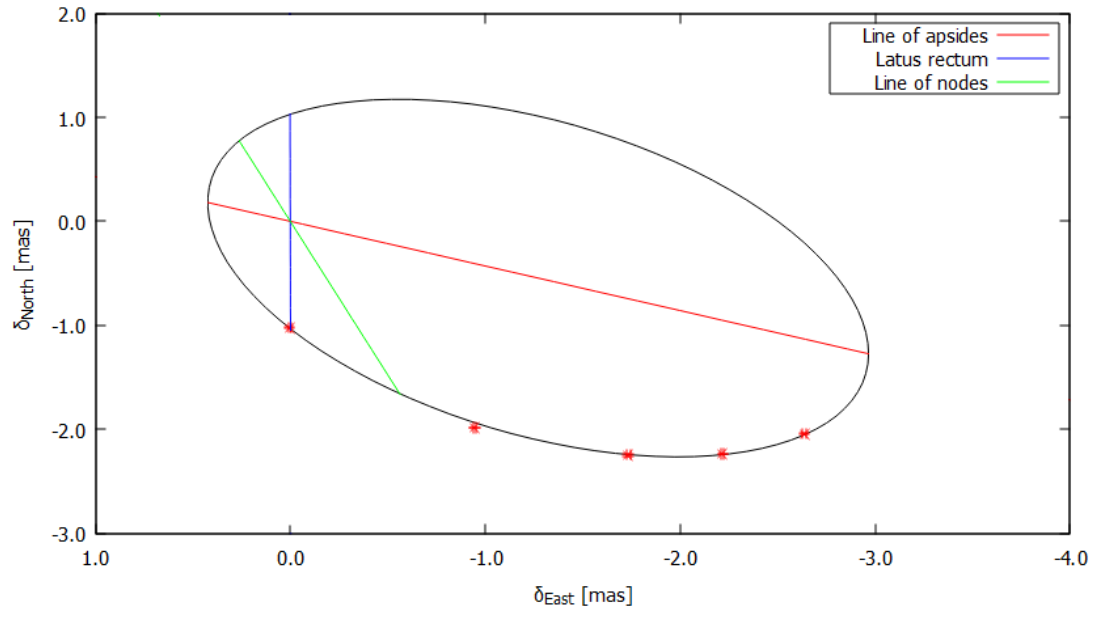$$M_3 = (19.2 \pm 3.8)\,\text{M}_\odot \tag{3.40}$$

Figure 3.18: The astrometric orbit of HD 152246

4. Delta Cir

The hierarchical triple system δ Cir (HD 135240, HIP 74778, HR 5664) consists of an eclipsing binary and a more distant third star. All three components are OB stars. The eclipsing binary has an eccentric orbit with period of 3.9 days. The third body and the binary orbit around a common center of gravity with estimated period of 1644 days [Mayer et al., 2014].

The first 3 radial velocities of this object were published by Campbell [1928]. Additional radial velocities were obtained by Feast et al. [1957], Buscombe and Kennedy [1965], Buscombe and Kennedy [1969] and Conti et al. [1977].

δ Cir is included in a catalog of Strömgren-Crawford uvbyβ photometry [Paunzen, 2015]. The TESS space telescope obtained two photometry segments of the system.

Astrometric measurements of δ Cir are listed in Table 4.1.

Walborn [1972] classified the object as O7.5 III (f), while Hiltner et al. [1969] assigned the spectral type O8.5. Maíz Apellániz et al. [2016] resolved only two components in the spectra and classified them as O7 IV (f) and B. Mayer et al. [2014] assigned the primary component a spectral type of O8 IV.

Thackeray and Emerson [1969] derived the orbit of the eclipsing binary for the first time. They published additional radial velocities as well. Orbital solutions were later derived also by Stickland et al. [1993] Penny et al. [2001] and Mayer et al. [2014]. Penny et al. [2001] analysed the International Ultraviolet Explorer (IUE) spectra and noticed the presence of a third body spectral lines.

The third body was confirmed interferometrically [Sana et al., 2014]. The interferometric observations were made in June 2012 by the PIONIER combiner at the four Auxiliary Telescopes of the ESO VLTI. The angular separation between the primary and the third component was $\rho = 3.78$ mas. Since then, several more interferometric observations were made.

Bagnulo et al. [2015] did not detect any magnetic field of the system. Southworth and Bowman [2022] tested the stars in the system for intrinsic variability, but they did not detect any significant independent pulsation mode. According to Shi et al. [2022] the TESS light curve of δ Cir has signs of eccentric eclipse and similar pulsating variations, but they were not able to find a frequency of the pulsation.

Table 4.1: Astrometry of Delta Cir [Gaia Collaboration, 2022].

Right ascension (J2016)	$\alpha = 15^{\text{h}}\,16^{\text{m}}\,56.887^{\text{s}}$
Declination (J2016)	$\delta = 60°57'26.180''$
Parallax	$p = (1.43 \pm 0.12)$ mas
Proper motion in α	$\mu_\alpha = (-4.09 \pm 0.11)$ mas/yr
Proper motion in δ	$\mu_\delta = (-3.76 \pm 0.13)$ mas/yr

Mayer et al. [2014] estimated that the period of mutual orbit of the eclipsing binary and the third body is 1644 days. Their orbital solution of δ Cir is summarized in Tables 4.2 and 4.3. They also showed that the line of apsides of the

binary rotates with period of about 141 years. They noted there are indications of lines of a fourth star in the spectra. It is thus possible that the third body is a binary as well.

Table 4.2: Spectroscopic elements of the system Delta Cir [Mayer et al., 2014].

Short orbit		Long orbit	
P (d)	3.902463	P	1644
T_p (RJD)	54285.639	T_p (RJD)	37484.0
e	0.068	e	0.416
ω_p (°)	307.1	ω_p (°)	284.0
K_1 (km.s^{-1})	156.8	K_{1+2} (km.s^{-1})	22.4
K_1/K_2	0.559	K_{1+2}/K_3	0.407
K_2 (km.s^{-1})	280.4	K_3 (km.s^{-1})	55.0

Table 4.3: Photometric elements of Delta Cir [Mayer et al., 2014].

Primary star		Secondary star	
Relative radius	0.265	Relative radius	0.165
T_eff (K)	34000	T_eff (K)	29000
M (M$_\odot$)	23.6	M (M$_\odot$)	13.2
R (R$_\odot$)	9.20	R (R$_\odot$)	5.73
M_bol	-7.76	M_bol	-6.05
$\log g$ (cgs)	3.88	$\log g$ (cgs)	4.04
L_V	0.6460	L_V	0.1877
$L_{\mathrm{H_p}}$	0.6485	$L_{\mathrm{H_p}}$	0.1852
L_3		0.1663	
i (°)		75.81	
a (R$_\odot$)		34.7	

4.1 Origin of the data

In this work I used 39 CHIRON spectra observed in 2021-2022, 95 HARPS spectra from 2009-2012, 29 FEROS spectra from 2007-2009 and 2 UVES spectra from 2000-2001. CHIRON, HARPS, FEROS and UVES are echelle spectrographs. CHIRON and FEROS are described in more detail in section 3.1. HARPS is a fibre-fed high resolution echelle spectrograph with resolution $R \sim$ 115 000 attached to the ESO 3.6m telescope in La Silla Obeservatory in Chile. UVES is a cross-dispersed echelle spectrograph connected to ESO's Very Large Telescope (VLT) at Cerro Paranal in Chile. Its resolving power is up to $R \sim 110$ 000 in visual section of a spectrum.

Next I analysed two light curves of δ Cir. The first light curve was obtained by the TESS (Transiting Exoplanet Survey Satellite). TESS is equipped with a

single instrument consisting of 4 wide field-of-view optical cameras. Each camera has 105 mm aperture, focal ratio $f/1.4$ and field of view $24° \times 24°$ [Vanderspek et al., 2021]. The light curve covers the time interval from May 2019 to June 2019 (RJD 58624.5-58652.4). The light curve was downloaded from Barbara A. Mikulski Archive for Space Telescopes (MAST): `https://archive.stsci.edu/`.

The second light curve of δ Cir was obtained by an instrument called FRAM. It is a robotic Schmidt-Cassegrain telescope with diameter of 305 mm located in Argentina at the Pierre Auger observatory at Los Leones. The photometry was observed via a f/2.8 photographic lens with focal length of 300 mm that is attached on the main tube of the telescope. The lens is used for wide field imaging with a CCD camera G4-16000. The instrument is equipped with UBVRI photometric filers.

The FRAM photometry of δ Cir was observed from December 2014 to May 2015 (RJD 57019.8-57145.7). A star map with δ Cir and its comparison and check stars used in FRAM photometry is shown in picture 4.1. I identified the comparison star as HD 135591 and the check stars as HD 135160, HD 135241 and HD 134657. Its visual magnitude is V=5.46 [Ducati, 2002].

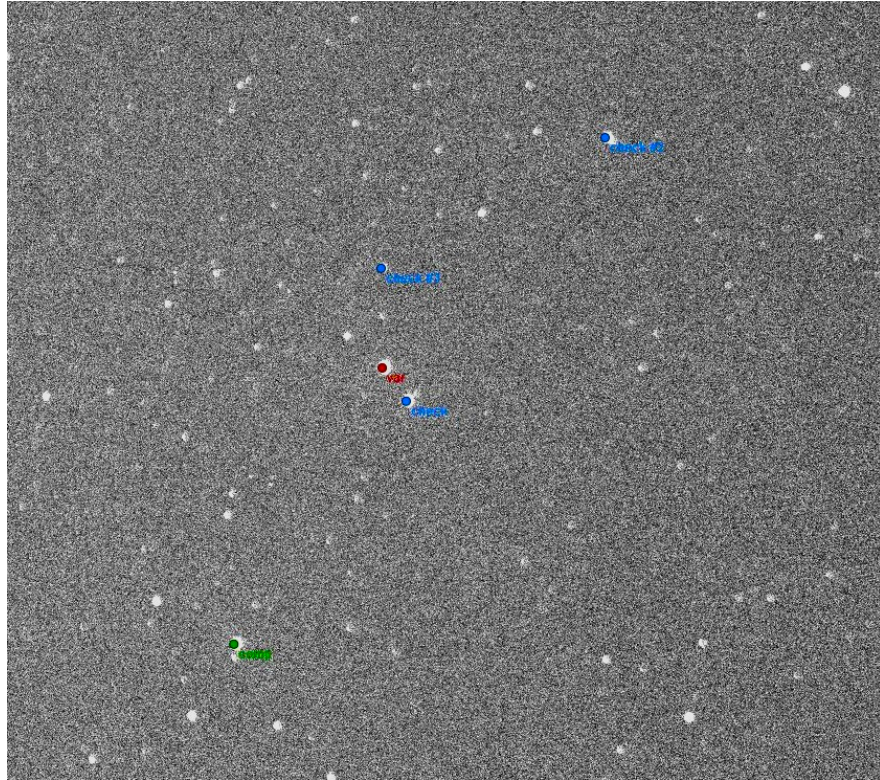Figure 4.1: Star map with δ Cir (red), comparison star HD 135591 (green) and check stars HD 135160, HD 135241 and HD 134657 (blue) used for FRAM photometry.

4.2   Methods and programs

I used the program ReSpefo to rectify the CHIRON spectra, which I had already received in the form of 1-D spectra. I used ReSpefo to measure radial velocities as well as and positions of telluric lines. All spectroscopic data were

analysed with programs KOREL and FOTEL. All of these programs are described in section 3.2.

To analyse the photometric data, I used the program Phoebe 1 (legacy). It is a software intended for modeling eclipsing binary stars. It is based on a program for binary star modeling developed by Wilson and Devinney [Wilson and Devinney, 1971]. Compared to the WD program, Phoebe has, for example, new algorithms for convergence and graphical user interface. The program together with user manual is available for free at `http://phoebe-project.org/1.0`. Another manual, suitable for beginners, is Zasche [2016]. The principles of eclipsing binary stars modeling in Phoebe is described in detail in Prša and Zwitter [2005].

I used program Period04 to search for frequencies in my data. Period04 is specifically intended for analysing time series of astronomical data containing gaps [Lenz and Breger, 2004]. The program uses discrete Fourier transform to search for frequencies in the data. It is written in Java/C++ and it is a reworked and improved version of an older program Period98. Period04 is available for free at `http://period04.net/`.

4.3 Results

4.3.1 Spectroscopy

First I tried to confirm the mutual orbital period of the third body and the eclipsing binary and evaluate it more precisely. The systemic velocity γ of the binary should change periodically due to the mutual orbital motion of the binary and the third body. The long orbital period is about 1640 days, so γ does not change significantly over the course of several days. The γ velocity can be easily determined by FOTEL when solving only for the orbit of the close binary. I split the CHIRON spectra into two sets according to their RJD. The first set has 11 spectra covering the time interval from RJD 59219.9 to RJD 59294.8. In the second set there are 28 spectra covering the time interval RJD 59615.9 to RJD 59692.7. I measured RVs of the primary star in ReSpefo on the four following suitable spectral lines (and the secondary, in case when its lines were visible)

- He II 4685.682 Å,

- He I 4921.931 Å,

- He I 5015.678 Å,

- He II 5411.516 Å.

Then I derived FOTEL solutions of the inner eclipsing binary for both sets of spectra. I did that with RVs measured on each of the 4 lines. All γ velocities I obtained from FOTEL are summarized in Table 4.4. Mayer et al. [2014] already did the same procedure with 13 more sets of RVs. All their and my two values of systemic velocities determined for each time interval are in Table 4.5.

Table 4.4: The systemic radial velocities γ of the eclipsing binary calculated by FOTEL.

line	4686	4922	5015	5411
γ [km/s] of set 1	13.2 ± 2.9	12.7 ± 2.1	19.2 ± 2.0	12.7 ± 37.6
γ [km/s] of set 2	3.9 ± 0.8	2.5 ± 5	4.9 ± 2.0	0.56 ± 0.5

Table 4.5: The systemic velocities γ determined for several sets of spectra covering short time intervals.

start [RJD]	end [RJD]	center [RJD]	center [year]	γ [km/s]	σ_γ [km/s]
39594	39723	39658.5	1967.7	9.2	12.3
44449	44460	44454.5	1980.2	17.5	9.9
48885	48894	48889.5	1992.8	-8.3	4.9
49867	49874	49870.5	1995.4	-0.7	9.5
50152	50155	50153.5	1996.2	-16.5	8.8
54277	54302	54289.5	2007.6	18.6	4.6
54660	54667	54663.5	2008.7	-0.8	4.9
55028	55031	55029.5	2009.6	-7.9	3.5
55360	55383	55371.5	2010.5	-14.7	2.4
55736	55762	55749.0	2011.6	29.5	3.2
56103	56113	56108.0	2012.5	13.6	2.7
56132	56136	56134.0	2012.6	9.5	2.2
59220	59295	59257.5	2021.1	14.5	3.2
59616	59693	59654.5	2022.2	3.0	1.9

I used the program Period04 to find the period of γ changes. The frequency corresponding to period 1643.53 days had the highest peak in the Fourier spectrum calculated by Period04. Then I tried to search for a more accurate period in FOTEL. I used the 1643.53 days as an initial estimate for FOTEL. I obtained the period $P_{\text{out}} = (1641.18 \pm 0.55)$ d.

I continued with disentangling the spectra with program KOREL. I created an input file for KOREL from all the the 39 CHIRON, 30 FEROS, 95 HARPS and 1 UVES (the second UVES spectrum was too noisy, so I did not use it) spectra. The process of generating the KOREL input file is described in detail in subsection 3.2.3.

The spectra made by different instruments cover different wavelengths and they overlap only on a small wavelength interval. Namely the CHIRON spectra cover the region from 450 nm to 890 nm and all of the HARPS, FEROS and UVES spectra, available to me from the original analysis by P. Mayer, cover only the wavelengths 430-475 nm.

I disentangled the spectral region around the line He II 4685.682 Å, the only suitable line in the wavelength interval where all the spectra overlap. As initial estimates of the orbital elements I used their values derived by Mayer et al. [2014] (see Table 4.2) except for the long period $P_{\text{out}} = 1641.18$ d.

It would also be possible to take the RVs measured in reSpefo and calculate the orbital elements in FOTEL. However, the elements as well as the RVs obtained from KOREL are much more reliable.

The orbital elements derived by KOREL are summarized in Table 4.6. The rate of apsidal precession corresponds to a period of 131 years, which is 10 years shorter than the period estimated by Mayer et al. [2014].

All the radial velocities determined by KOREL are summarized in Table A.5. The phase diagrams for RVs on the long orbit is shown in Figure 4.2. I will come back later to the phase diagram for the motion on the short orbit.

The residuals of third star's radial velocities are large, even up to 80 km.s^{-1} (see Figure 4.2). This might be caused be the presence of a fourth component in the system - the third body could actually be a binary. The same idea was suggested by Mayer et al. [2014] who tried to fit spectral lines of δ Cir with Gaussians. The quality of their fit with three and four Gaussians was quite comparable.

The disentangled line He II 4685.682 is shown in Figure 4.3. Apart from this line there are two more lines visible on the left and right side of the He line of the secondary and third star. These are probably the lines of oxygen O II 4676.2, O II 4698.5 and O II 4699.2 which are more pronounced for the B type secondary and tertiary.

Table 4.6: KOREL solution of δ Cir for the line He II 4685.682 Å

Element	Value
Short orbit	
P (d)	3.90275781
T_{p} (RJD)	59249.742
e	0.058
ω_{p} (°)	324.67
K_1 (km.s^{-1})	159
q (km.s^{-1}.100yr^{-1})	0.576
K_2 (km.s^{-1})	276
$\dot{\omega}_{\mathrm{p}}$ (°.d^{-1})	0.0075
Long orbit	
P (d)	1641.18
T_{p} (RJD)	58943.0
e	0.417
ω_{p} (°)	302.2
K_{1+2} (km.s^{-1})	20.7
q	0.48
K_3 (km.s^{-1})	42.8
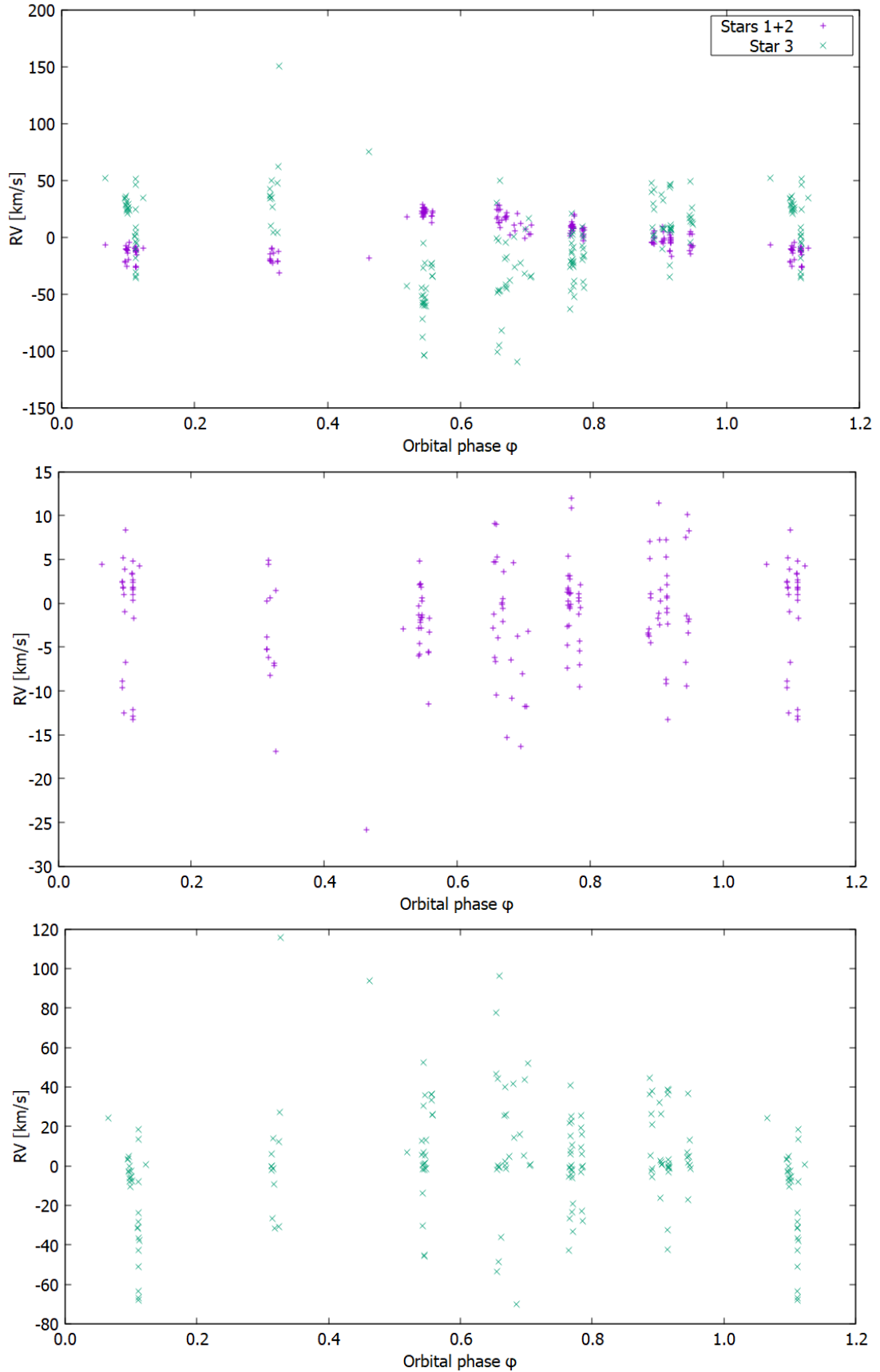
Figure 4.2: Top figure: Phase diagram for radial velocities of the center of mass of inner binary and the third star on the long orbit. Gamma velocity of the system is already subtracted. Middle figure: RV residuals for the center of mass of the binary. Bottom figure: RV residuals for the third component.
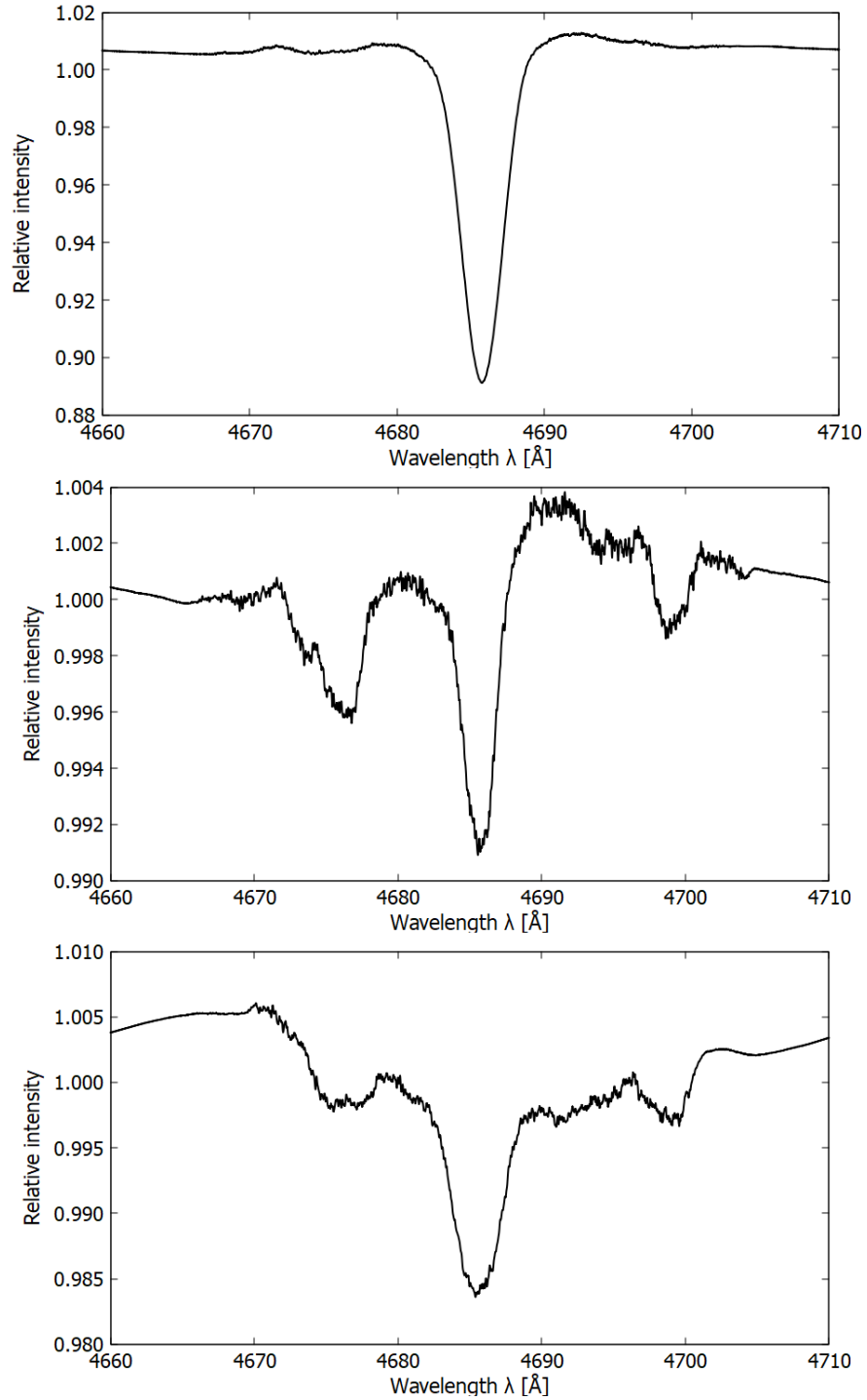
Figure 4.3: Disentangled spectral line He II 4685.682 Å. Line of the primary star is in the top figure, secondary star in the middle figure and third star in the bottom figure. Lines of oxygen O II 4676.2, O II 4698.5 and O II 4699.2 are visible on the left and right hand side of the He line of the secondary and third star.

4.3.2 Photometry

Phoebe is able to fit both light curves and radial velocity curves. To calculate the parameters of the eclipsing binary in Phoebe, I applied the following

approach. I used the radial velocities of the primary and secondary from the KOREL solution together with the densely covered light curves from TESS and FRAM. I started with the elements from Mayer et al. [2014] study. I set the gravity brightening coefficients and the albedos to 1, because all the stars of δ Cir are hot stars, used the linear limb darkening coefficients, and allowed calculation of the contribution of the third light. The convergency went well and the results are summarised in Table 4.7. Both light curves and the radial velocity curve are shown in Figures 4.4, 4.5 and 4.6.

Since the FRAM and TESS light curves are densely covered by data points, I was able to obtain more precise values of the relative radii and the temperature of the secondary star. When comparing with tables in Harmanec [1988] the parameters of the primary are closest to spectral type O8 V. I got the same result when comparing with the tables in Martins et al. [2005]. The parameters of the secondary star are most similar to parameters of stars with spectral type B0.5 V [Harmanec, 1988].

Table 4.7: Phoebe solution of δ Cir light curve. The epoch of primary minimum is RJD = 59 625.674167.

| Parameter	Value	Parameter	Value
a (R$_\odot$)	34.26 ± 0.18	M_1 (M$_\odot$)	22.53
e	0.0620 ± 0.0013	M_2 (M$_\odot$)	12.95
$\Delta\phi$	-0.24443 ± 0.00016	R_1 (R$_\odot$)	9.68
ω_p (°)	336.7 ± 2.9	R_2 (R$_\odot$)	4.97
γ (km.s^{-1})	3.10 ± 0.68	M_{bol_1} (mag)	-7.89
i (°)	77.36 ± 0.11	M_{bol_2} (mag)	-5.58
q	0.5748 ± 0.0035	$\log g_1$ (cgs)	3.82
$T_{\mathrm{eff},2}$ (K)	$27\ 860 \pm 170$	$\log g_2$ (cgs)	4.16
L_1 (TESS)	0.6059	L_1 (FRAM)	0.6933
L_2 (TESS)	0.1078	L_2 (FRAM)	0.122
L_3 (TESS)	0.2863 ± 0.0029	L_3 (FRAM)	0.1847 ± 0.0023
$(R_1/a)_\mathrm{pole}$	0.27712 ± 0.00098	$(R_1/a)_\mathrm{pole}$	0.14388 ± 0.00089
$(R_1/a)_\mathrm{side}$	0.2915 ± 0.0012	$(R_1/a)_\mathrm{side}$	0.14607 ± 0.00095
$(R_1/a)_\mathrm{point}$	0.2819 ± 0.0010	$(R_1/a)_\mathrm{point}$	0.14447 ± 0.00091
$(R_1/a)_\mathrm{back}$	0.2878 ± 0.0011	$(R_1/a)_\mathrm{back}$	0.14576 ± 0.00094
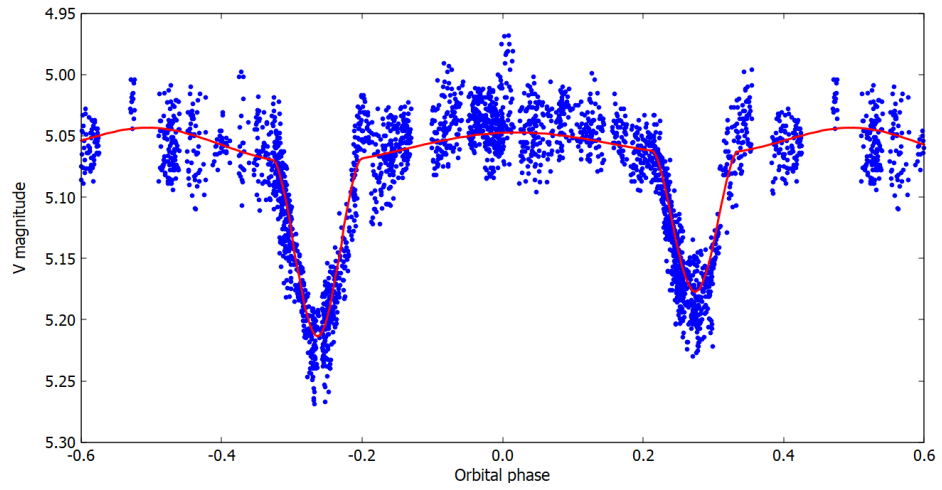
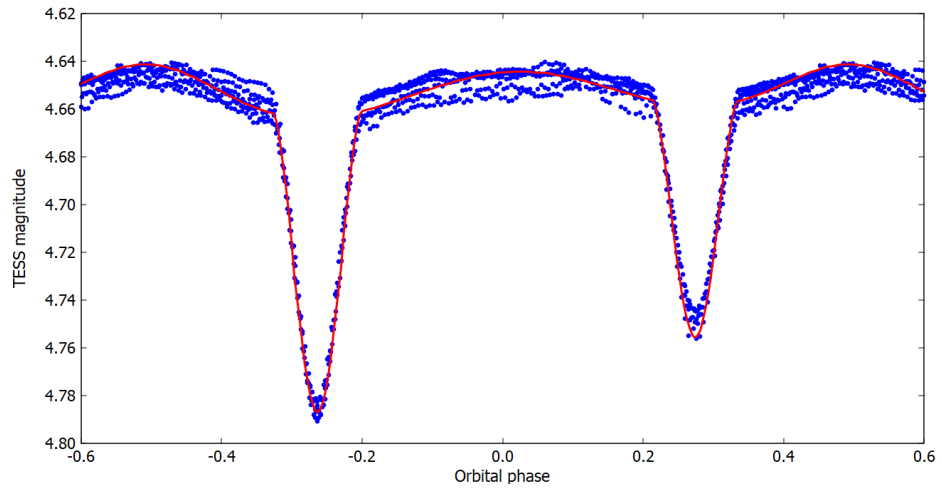Figure 4.4: Comparison of observed and calculated light curves of FRAM photometry.

Figure 4.5: Comparison of observed and calculated light curves of TESS photometry.
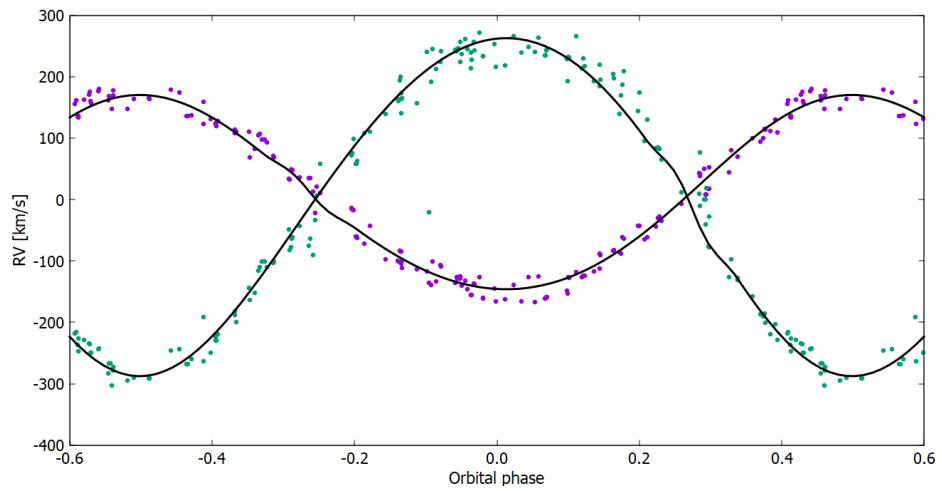
Figure 4.6: Measured and calculated radial velocity curve of the eclipsing binary.

Conclusion

I processed spectra of the system HD 152246 from spectrographs CHIRON and HERCULES measured in years 2021 and 2022. Using the method of spectra disentangling I showed that the outer orbit eccentricity of HD 152246 is lower than predicted. Its value is only $e_{\rm out} = 0.75$. In addition to the eccentricity I calculated also other orbital elements more accurately and precisely. Apart from the new spectra from years 2021/2022 I used older spectra from years 1999-2013 measured by spectrographs FEROS and BESO.

I proved that the radial velocity semi-amplitude K_1 of the primary on the short inner orbit is changing. This implies that the inclination of the inner orbit is changing as well. There are also hints that the inclination of the long outer orbit is changing as well, albeit at a much slower rate. It is possible that the inclinations of both inner and outer orbit are changing periodically in time. To confirm this assumption, it is necessary to obtain more spectra. New spectroscopic measurements are already planned for the time period around the closest periastron passage which should happen on 5th August 2023 (RJD 60162.23). Apart from spectroscopic data I also analysed interferometric measurements of the system. I used the Thiele-Innes constants to fit the astrometric orbit. In addition to the orbital elements I calculated the dynamical parallax of the object and masses of its components.

I processed measurements od the system δ Cir from spectrograph CHIRON from years 2021 and 2022. I calculated systemic radial velocities of the eclipsing binary for two groups of spectra covering shorter time intervals. Then I used my two values together with several already published systemic velocities to determine the long orbital period of the binary and the third body. I obtained the values of orbital elements for both the long and short orbit via spectra disentangling in the program KOREL. I also analysed light curves of the eclipsing binary together with its RV curves and calculated more precise parameters of its two components.

Bibliography

S. Bagnulo, L. Fossati, J. D. Landstreet, and C. Izzo. The FORS1 catalogue of stellar magnetic field measurements. *Astronomy & Astrophysics*, 583:A115, November 2015. doi: 10.1051/0004-6361/201526497.

T. Borkovits, T. Hajdu, J. Sztakovics, S. Rappaport, A. Levine, I. B. Bíró, and P. Klagyivik. A comprehensive study of the Kepler triples via eclipse timing. *Monthly Notices of the Royal Astronomical Society*, 455(4):4136–4165, February 2016. doi: 10.1093/mnras/stv2530.

William Buscombe and P. Morris Kennedy. Radial velocities of 200 southern B stars. *Monthly Notices of the Royal Astronomical Society*, 130:281, January 1965. doi: 10.1093/mnras/130.4.281.

William Buscombe and Pamela M. Kennedy. Radial velocities of southern OB stars and supergiants. *Monthly Notices of the Royal Astronomical Society*, 143: 1, January 1969. doi: 10.1093/mnras/143.1.1.

W. W. Campbell. Catalogue of observed velocities. *Publications of Lick Observatory*, 16:1–346, January 1928.

P. S. Conti, E. M. Leep, and J. J. Lorre. Spectroscopic studies of O-type stars. VIII. Radial velocities and the K-term. *Astrophysical Journal*, 214:759–772, June 1977. doi: 10.1086/155305.

J. Dachs, D. Kaiser, A. Nikolov, and W. A. Sherwood. UBV-Hβ photometry of luminous stars between l=335 and l=6. *The Astrophysical Journal Supplement Series*, 50:261–275, November 1982.

J. R. Ducati. VizieR Online Data Catalog: Catalogue of Stellar Photometry in Johnson's 11-color system. *VizieR Online Data Catalog*, January 2002.

M. W. Feast, A. D. Thackeray, and A. J. Wesselink. Radial velocities of southern B stars determined at the Radcliffe Observatory Part II. *Memoirs of the Royal Astronomical Society*, 68:1–35, January 1957.

L. Fossati, N. Castro, M. Schöller, S. Hubrig, N. Langer, T. Morel, M. Briquet, A. Herrero, N. Przybilla, H. Sana, F. R. N. Schneider, A. de Koter, and BOB Collaboration. B fields in OB stars (BOB): Low-resolution FORS2 spectropolarimetry of the first sample of 50 massive stars. *Astronomy & Astrophysics*, 582:A45, October 2015. doi: 10.1051/0004-6361/201526725.

Gaia Collaboration. Gaia Data Release 3: Summary of the content and survey properties. *arXiv e-prints*, page arXiv:2208.00211, July 2022.

R. F. Garrison, W. A. Hiltner, and R. E. Schild. MK spectral classification for southern OB stars. *The Astrophysical Journal Supplement Series*, 35:111–126, September 1977. doi: 10.1086/190468.

P. Hadrava. Orbital elements of multiple spectroscopic stars. *Astronomy and Astrophysics Supplement*, 114:393, December 1995.

P. Hadrava. FOTEL 4 - User's guide. *Publications of the Astronomical Institute of the Czechoslovak Academy of Sciences*, 92:1–14, January 2004a.

P. Hadrava. KOREL – User's guide. In *Publications of the Astronomical Institute of the Czechoslovak Academy of Sciences*, volume 92, pages 15–35, January 2004b.

P. Hadrava. Disentangling of spectra - theory and practice. *arXiv e-prints*, page arXiv:0909.0172, September 2009. doi: 10.48550/arXiv.0909.0172.

P. Harmanec. Stellar Masses and Radii Based on Modern Binary Data. *Bulletin of the Astronomical Institutes of Czechoslovakia*, 39:329, December 1988.

W. A. Hiltner, R. F. Garrison, and R. E. Schild. MK Spectral Types for Bright Southern OB Stars. *The Astrophysical Journal*, 157:313, July 1969. doi: 10. 1086/150069.

Lea A. Hirsch, Lee Rosenthal, Benjamin J. Fulton, Andrew W. Howard, David R. Ciardi, Geoffrey W. Marcy, Eric Nielsen, Erik A. Petigura, Robert J. de Rosa, Howard Isaacson, Lauren M. Weiss, Evan Sinukoff, and Bruce Macintosh. Understanding the Impacts of Stellar Companions on Planet Formation and Evolution: A Survey of Stellar and Planetary Companions within 25 pc. *The Astronomical Journal*, 161(3):134, March 2021. doi: 10.3847/1538-3881/abd639.

E. Høg, C. Fabricius, V. V. Makarov, S. Urban, T. Corbin, G. Wycoff, U. Bastian, P. Schwekendiek, and A. Wicenec. The Tycho-2 catalogue of the 2.5 million brightest stars. *Astronomy & Astrophysics*, 355:L27–L30, March 2000.

G. Holgado, S. Simón-Díaz, L. Haemmerlé, D. J. Lennon, R. H. Barbá, M. Cerviño, N. Castro, A. Herrero, G. Meynet, and J. I. Arias. The IACOB project. VI. On the elusive detection of massive O-type stars close to the ZAMS. *Astronomy & Astrophysics*, 638:A157, June 2020. doi: 10.1051/0004-6361/202037699.

S. Hubrig, S. P. Järvinen, I. Ilyin, M. Schöller, and R. Jayaraman. Are magnetic fields universal in O-type multiple systems? *Monthly Notices of the Royal Astronomical Society*, 521(4):6228–6246, June 2023. doi: 10.1093/mnras/stad730.

J. Juryšek, P. Zasche, M. Wolf, J. Vraštil, D. Vokrouhlický, M. Skarka, J. Liška, J. Janík, M. Zejda, P. Kurfürst, and E. Paunzen. New inclination changing eclipsing binaries in the Magellanic Clouds. *Astronomy & Astrophysics*, 609: A46, January 2018. doi: 10.1051/0004-6361/201730655.

H. Karttunen, P. Krüger, H. Oja, M. Poutanen, and K.J. Donner. *Fundamental Astronomy*. Fifth Edition. Springer, Berlin, 2007. ISBN 978-3-540-34143-7.

G. Klare and T. Neckel. UBV, Hβ and polarization measurements of 1660 southern OB stars. *Astronomy & Astrophysics, Suppl. Ser.*, 27:215–248, February 1977.

J. B. Le Bouquin, J. P. Berger, B. Lazareff, G. Zins, P. Haguenauer, L. Jocou, P. Kern, R. Millan-Gabet, W. Traub, O. Absil, J. C. Augereau, M. Benisty,

N. Blind, X. Bonfils, P. Bourget, A. Delboulbe, P. Feautrier, M. Germain, P. Gitton, D. Gillier, M. Kiekebusch, J. Kluska, J. Knudstrup, P. Labeye, J. L. Lizon, J. L. Monin, Y. Magnard, F. Malbet, D. Maurel, F. Ménard, M. Micallef, L. Michaud, G. Montagnier, S. Morel, T. Moulin, K. Perraut, D. Popovic, P. Rabou, S. Rochat, C. Rojas, F. Roussel, A. Roux, E. Stadler, S. Stefl, E. Tatulli, and N. Ventura. PIONIER: a 4-telescope visitor instrument at VLTI. *Astronomy & Astrophysics*, 535:A67, November 2011. doi: 10.1051/0004-6361/201117586.

G Ledrew. The real starry sky. *Journal of the Royal Astronomical Society of Canada*, 95:32, 2001.

P. Lenz and M. Breger. Period04: A software package to extract multiple frequencies from real data. In *Proceedings of the International Astronomical Union*, volume 224, pages 786–790. Cambridge University Press, December 2004. doi: 10.1017/S1743921305009750.

Tullio Levi-Civita. Astronomical consequences of the relativistic two-body problem. *American Journal of Mathematics*, 59(2):225–234, 1937.

L. B. Lucy. Mass estimates for visual binaries with incomplete orbits. *Astronomy & Astrophysics*, 563:A126, March 2014. doi: 10.1051/0004-6361/201322649.

J. Maíz Apellániz, A. Sota, J. I. Arias, R. H. Barbá, N. R. Walborn, S. Simón-Díaz, I. Negueruela, A. Marco, J. R. S. Leão, A. Herrero, R. C. Gamen, and E. J. Alfaro. The Galactic O-Star Spectroscopic Survey (GOSSS). III. 142 Additional O-type Systems. *The Astrophysical Journal Supplement Series*, 224 (1):4, May 2016. doi: 10.3847/0067-0049/224/1/4.

Rosemary A. Mardling and Sverre J. Aarseth. Tidal interactions in star cluster simulations. *Monthly Notices of the Royal Astronomical Society*, 321:398–420, March 2001. doi: 10.1046/j.1365-8711.2001.03974.x.

F. Martins, D. Schaerer, and D. J. Hillier. A new calibration of stellar parameters of Galactic O stars. *Astronomy & Astrophysics*, 436(3):1049–1065, June 2005. doi: 10.1051/0004-6361:20042386.

P. Mayer, P. Harmanec, H. Sana, and J.-B. Le Bouquin. The Three-body System δ Circini. *The Astronomical Journal*, 148:114, dec 2014. doi: 10.1088/0004-6256/148/6/114.

W. W. Morgan, A. D. Code, and A. E. Whitford. Studies in Galactic STRUCTURE.II.LUMINOSITY Classification for 1270 Blue Giant Stars. *Astrophysical Journal Supplement*, 2:41, July 1955. doi: 10.1086/190016.

A. Nasseri, Chini, R., Harmanec, P., Mayer, P., Nemravová, J. A., Dembsky, T., Lehmann, H., Sana, H., and Le Bouquin, J.-B. Hd246: a new high-mass triple system and its basic properties. *Astronomy & Astrophysics*, 568:A94, July 2014. doi: 10.1051/0004-6361/201424382.

E. Paunzen. A new catalogue of Strömgren-Crawford uvbyβ photometry. *Astronomy & Astrophysics*, 580:A23, aug 2015. doi: 10.1051/0004-6361/201526413.

Laura R. Penny, Debra Seyle, Douglas R. Gies, James A. Harvin, Jr. Bagnuolo, William G., M. L. Thaller, A. W. Fullerton, and L. Kaper. Tomographic Separation of Composite Spectra. VII. The Physical Properties of the Massive Triple System HD 135240 (δ Circini). *The Astrophysical Journal*, 548:889–899, feb 2001. doi: 10.1086/319031.

A. Prša and T. Zwitter. A Computational Guide to Physics of Eclipsing Binaries. I. Demonstrations and Perspectives. *The Astrophysical Journal*, 628(1):426–438, July 2005. doi: 10.1086/430591.

H. P. Robertson. Note on the preceding paper: The two body problem in general relativity. *Annals of Mathematics*, 39(1):101–104, 1938.

H. Sana. The multiplicity of massive stars: a 2016 view. In J. J. Eldridge, J. C. Bray, L. A. S. McClelland, and L. Xiao, editors, *The Lives and Death-Throes of Massive Stars*, volume 329, pages 110–117, November 2017. doi: 10.1017/S1743921317003209.

H. Sana, J. B. Le Bouquin, S. Lacour, J. P. Berger, G. Duvert, L. Gauchet, B. Norris, J. Olofsson, D. Pickel, G. Zins, O. Absil, A. de Koter, K. Kratter, O. Schnurr, and H. Zinnecker. Southern Massive Stars at High Angular Resolution: Observational Campaign and Companion Detection. *The Astrophysical Journal Supplement Series*, 215(1):15, nov 2014. doi: 10.1088/0067-0049/215/1/15.

R. E. Schild, R. F. Garrison, and W. A. Hiltner. UBV Photometry for southern OB stars. *The Astrophysical Journal Supplement Series*, 51:321–336, April 1983. doi: 10.1086/190852.

Rudolph E. Schild, W. A. Hiltner, and N. Sanduleak. A Spectroscopic Study of the Association Scorpius OB 1. *Astrophysical Journal*, 156:609, May 1969. doi: 10.1086/149992.

Xiang-dong Shi, Sheng-bang Qian, and Lin-Jia Li. New Pulsating Stars Detected in EA-type Eclipsing-binary Systems Based on TESS Data. *The Astrophysical Journal Supplement Series*, 259(2):50, April 2022.

A. Sota, J. Maíz Apellániz, N. I. Morrell, R. H. Barbá, N. R. Walborn, R. C. Gamen, J. I. Arias, and E. J. Alfaro. The Galactic O-Star Spectroscopic Survey (GOSSS). II. Bright Southern Stars. *The Astrophysical Journal Supplement*, 211(1):10, mar 2014. doi: 10.1088/0067-0049/211/1/10.

John Southworth and Dominic M. Bowman. High-mass pulsators in eclipsing binaries observed using TESS. *Monthly Notices of the Royal Astronomical Society*, 513(3):3191–3209, July 2022. doi: 10.1093/mnras/stac875.

T. E. Sterne. Apsidal motion in binary stars. *Monthly Notices of the Royal Astronomical Society*, 99:451–462, March 1939. doi: 10.1093/mnras/99.5.451.

M. F. Sterzik and A. A. Tokovinin. Relative orientation of orbits in triple stars. *Astronomy & Astrophysics*, 384:1030–1037, March 2002. doi: 10.1051/0004-6361:20020105.

D. J. Stickland and C. Lloyd. Spectroscopic binary orbits from ultraviolet radial velocities. Paper 31: Stars with few IUE observations. *The Observatory*, 121: 1–54, February 2001.

D. J. Stickland, R. H. Koch, I. Pachoulakis, and R. J. Pfeiffer. Spectroscopic binary orbits from ultraviolet radial velocities. Paper 11: delta Circini (HD 135240). *The Observatory*, 113:139–144, jun 1993.

A. D. Thackeray and B. Emerson. Orbits of two O-type spectroscopic binaries HD 93403 and 135240. *Monthly Notices of the Royal Astronomical Society*, 142: 429, jan 1969. doi: 10.1093/mnras/142.4.429.

A. D. Thackeray, S. B. Tritton, and E. N. Walker. Radial velocities of southern B stars determined at the Radcliffe Observatory—VII. *Memoirs of the Royal Astronomical Society*, 77:199, January 1973.

A. Tokovinin. Statistics of multiple stars. In Christine Allen and Colin Scarfe, editors, *Revista Mexicana de Astronomia y Astrofisica Conference Series*, volume 21 of *Revista Mexicana de Astronomia y Astrofisica Conference Series*, pages 7–14, August 2004.

A. Tokovinin. Dynamics of Multiple Stars: Observations. In Nicole St. -Louis and Anthony F. J. Moffat, editors, *Massive Stars in Interactive Binaries*, volume 367 of *Astronomical Society of the Pacific Conference Series*, page 615, January 2007.

A. Tokovinin. The Updated Multiple Star Catalog. *The Astrophysical Journal Supplement Series*, 235(1):6, March 2018. doi: 10.3847/1538-4365/aaa1a5.

A. Tokovinin. Architecture of Hierarchical Stellar Systems and Their Formation. *Universe*, 7(9):352, September 2021. doi: 10.3390/universe7090352.

Andrei Tokovinin. From Binaries to Multiples. I. Data on F and G Dwarfs within 67 pc of the Sun. *The Astronomical Journal*, 147(4):86, April 2014. doi: 10. 1088/0004-6256/147/4/86.

R. Vanderspek, J. P. Doty, M. Fausnaugh, J. N. Villaseñor, J. M. Jenkins, Z. K. Berta-Thompson, C. J. Burke, and G. R. Ricker. Tess instrument handbook, December 2021. Available online at `https://archive.stsci.edu/files/ live/sites/mast/files/home/missions-and-data/active-missions/ tess/_documents/TESS_Instrument_Handbook_v0.1.pdf`.

E. A. Vitrichenko, D. K. Nadyozhin, and T. L. Razinkova. Mass-luminosity relation for massive stars. *Astronomy Letters*, 33(4):251–258, April 2007. doi: 10.1134/S1063773707040044.

P. Škoda and P. Hadrava. Fourier Disentangling Using the Technology of Virtual Observatory. In A. Prša and M. Zejda, editors, *Binaries - Key to Comprehension of the Universe*, volume 435 of *Astronomical Society of the Pacific Conference Series*, page 71, December 2010.

P. Škoda, P. Hadrava, and J. Fuchs. VO-KOREL: A Fourier Disentangling Service of the Virtual Observatory. In Mercedes T. Richards and Ivan Hubeny, editors, *From Interacting Binaries to Exoplanets: Essential Modeling Tools*, volume 282, pages 403–404, April 2012.

N. R. Walborn. The space distribution of the O stars in the solar neighborhood. *Astronomical Journal*, 78:1067–1083, December 1973. doi: 10.1086/111509.

N.R. Walborn. Spectral Classification of OB Stars in Both Hemispheres and the Absolute-Magnitude Calibration. *The Astronomical Journal*, 77:312–318, may 1972. doi: 10.1086/111285.

Robert E. Wilson and Edward J. Devinney. Realization of Accurate Close-Binary Light Curves: Application to MR Cygni. *The Astrophysical Journal*, 166:605, June 1971. doi: 10.1086/150986.

P. Zasche. PHOEBE - step by step manual. *Open European Journal on Variable Stars*, 176:10, March 2016.

List of Figures

List of Tables

A. Attachments

A.1 Measured radial velocities of HD 152246

Table A.1: List of RVs of HD 152246 measured by KOREL and in reSpefo

	KOREL				reSpefo			
RJD	RV_1	σ_{RV_1}	RV_3	σ_{RV_3}	RV_1	σ_{RV_1}	RV_3	σ_{RV_3}
	km.s^{-1}	km.s^{-1}	km.s^{-1}	km.s^{-1}	km.s^{-1}	km.s^{-1}	km.s^{-1}	km.s^{-1}
59280.9091	17.513	1.469	33.966	13.364	0.097	1.442	29.143	12.588
59286.8044	20.833	3.764	34.364	5.989	6.577	3.328	26.757	11.682
59289.8894	-69.728	2.373	27.129	8.327	-81.953	2.595	8.320	10.159
59314.7703	-30.722	1.725	18.961	4.992	-45.690	1.905	6.150	13.395
59314.8815	-25.782	3.228	20.316	3.273	-41.323	1.948	8.577	14.306
59318.7526	-57.232	1.068	20.734	3.758	-72.187	2.805	4.810	6.705
59318.8508	-59.076	1.747	19.157	3.658	-74.247	2.786	-0.030	12.745
59319.7236	-62.936	1.229	18.604	4.074	-77.940	1.103	3.287	10.246
59319.8769	-61.641	0.651	19.237	1.829	-76.470	1.943	-4.697	16.090
59320.7030	-32.923	1.540	17.625	4.713	-50.183	2.623	3.070	19.457
59320.8699	-24.172	1.144	17.473	2.665	-39.277	1.437	11.100	21.818
59321.7254	15.414	1.614	15.759	3.514	-3.320	2.995	7.013	15.037
59321.8874	21.535	1.844	17.268	2.282	2.410	3.007	6.057	19.383
59322.7376	34.991	1.666	17.019	2.901	16.810	3.152	11.243	14.278
59322.8707	31.575	1.197	18.440	3.702	12.583	3.109	11.653	15.269
59324.6994	-52.986	3.088	16.411	4.140	-69.257	2.315	3.510	11.568
59324.8464	-60.012	1.110	16.877	2.100	-75.007	1.786	8.247	17.342
59327.7091	15.193	1.717	14.825	4.200	-2.870	1.890	5.840	14.819
59327.8939	23.472	0.924	13.382	5.223	4.413	0.777	8.127	14.983
59329.6799	-1.559	1.663	16.664	1.711	-18.017	2.925	9.500	19.103
59329.8534	-12.441	1.301	16.176	3.284	-29.357	1.607	7.120	18.061
59330.6567	-50.710	1.730	14.200	5.413	-66.140	1.054	4.147	13.045
59330.8165	-56.331	0.967	15.604	3.638	-72.020	1.496	0.057	12.708
59360.5848	-41.527	1.013	14.543	11.046	-56.100	2.986	-3.930	21.514
59360.6849	-44.252	1.197	7.422	3.328	-60.467	1.508	-10.130	20.886
59360.7835	-48.107	1.492	12.690	9.128	-63.410	2.402	-9.067	23.524
59361.5774	-54.339	0.806	7.082	3.028	-70.607	2.158	-9.313	24.853
59361.6919	-55.550	1.201	12.333	8.777	-69.723	0.999	-8.733	22.625
59361.7918	-52.519	1.619	9.553	6.711	-66.967	1.796	-14.300	29.602
59363.6080	18.983	1.017	6.144	4.698	-0.037	2.128	4.947	15.225
59363.7135	22.706	1.558	9.664	6.886	4.017	2.650	4.000	17.837
59363.8097	26.821	1.173	7.661	1.591	6.790	2.184	-3.497	26.090
59364.5770	47.414	1.727	8.980	5.033	27.520	4.265	0.613	26.835
59364.6784	48.010	0.961	8.311	2.281	28.263	4.388	6.793	16.012
59364.8740	44.225	1.306	10.518	5.056	24.617	3.843	8.007	14.399
59410.5335	-25.404	1.207	0.354	1.315	-41.967	1.813	-6.820	18.025
59410.6288	-20.688	0.327	2.028	4.178	-37.860	1.759	-5.660	15.499
59410.7174	-17.361	0.967	0.481	2.733	-36.397	0.185	-4.353	14.980
59411.5332	20.985	2.634	-0.955	4.819	1.417	1.400	-3.623	14.664
59411.6250	27.350	0.990	-0.801	3.716	7.357	3.960	0.503	13.466
59411.7047	29.559	0.859	-1.205	3.129	10.390	3.179	-4.950	9.972
59412.5641	54.717	0.723	-0.844	4.411	34.553	2.483	2.630	14.670
59412.6174	54.554	0.946	-0.713	4.631	33.297	3.995	3.530	17.789
59412.6782	53.991	0.683	0.891	3.943	34.307	4.879	5.167	14.025
59413.5376	24.460	1.675	-1.637	1.994	6.633	2.715	0.313	13.032
59413.6125	21.305	0.937	-1.797	4.216	2.913	3.070	-3.597	13.340

Table A.1: List of RVs of HD 152246 measured by KOREL and in reSpefo, continued

RJD	KOREL				reSpefo			
	RV_1	σ_{RV_1}	RV_3	σ_{RV_3}	RV_1	σ_{RV_1}	RV_3	σ_{RV_3}
	km.s^{-1}	km.s^{-1}	km.s^{-1}	km.s^{-1}	km.s^{-1}	km.s^{-1}	km.s^{-1}	km.s^{-1}
59413.6965	16.774	1.771	-1.422	3.845	-3.200	2.537	-0.950	16.422
59414.5063	-27.528	1.145	-3.062	4.753	-44.097	1.603	-10.570	12.547
59414.5888	-30.485	1.250	-2.473	4.436	-46.220	1.218	-9.043	10.594
59414.6750	-34.131	0.953	0.358	2.096	-50.743	1.782	-6.370	12.353
59415.5382	-46.655	0.974	-1.000	3.129	-63.500	1.730	-9.897	14.064
59415.6123	-46.592	1.101	-1.391	3.825	-63.433	2.206	-6.220	16.095
59415.6810	-46.104	0.940	-1.860	2.705	-61.673	1.052	-5.453	20.283
59421.5050	-46.308	3.092	-0.565	2.438	-60.460	2.215	-2.813	9.409
59421.5992	-45.302	0.888	-3.321	3.758	-60.320	0.677	-10.137	13.026
59421.7211	-43.723	1.455	-2.288	1.561	-61.697	3.733	-3.143	16.241
59424.5191	55.951	1.496	-2.474	2.489	35.963	5.022	2.757	11.825
59424.5930	57.980	2.698	1.479	10.657	35.490	3.011	5.280	16.733
59424.6620	55.947	0.740	-1.244	2.513	34.093	4.144	5.467	16.289
59432.4624	-21.923	1.550	-4.728	2.820	-40.050	0.952	-9.570	10.986
59432.5594	-26.403	1.251	-3.895	2.968	-43.120	1.816	-4.643	13.649
59432.6477	-30.338	1.405	-1.992	3.717	-46.213	1.919	-3.040	22.675
59472.4762	62.175	0.780	-8.440	0.487	40.293	3.846	-14.880	23.181
59472.4811	61.918	1.530	-9.533	0.963	40.990	4.826	-13.947	20.327
59472.5703	63.377	1.717	-12.411	3.087	42.057	3.976	-15.117	17.190
59473.4734	40.212	0.961	-9.327	1.810	20.200	2.778	-15.257	20.239
59473.5600	34.584	2.006	-9.418	2.652	13.870	3.363	-10.710	20.729
59474.4737	-15.325	0.466	-8.762	3.010	-33.263	2.513	-18.740	16.367
59474.5324	-18.490	0.540	-11.303	3.014	-35.227	3.623	-14.330	15.005
59475.4743	-38.696	0.895	-9.888	0.702	-56.513	2.484	-13.453	18.212
59475.5498	-39.203	1.122	-12.028	3.311	-53.967	2.398	-16.870	26.275
59476.4746	-18.827	2.473	-11.765	4.298	-38.113	0.512	-18.177	18.369
59476.5340	-16.512	0.856	-10.012	4.141	-34.113	2.546	-15.473	17.077
59477.4744	26.313	1.950	-12.911	2.844	7.003	3.830	-9.580	15.681
59477.5278	28.089	1.028	-10.759	6.398	6.420	4.291	-13.273	26.240
59480.4792	-14.315	2.260	-12.012	2.886	-32.713	1.951	-16.163	16.385
59480.5399	-17.065	1.490	-10.951	1.308	-34.457	2.162	-12.300	22.424
59481.5089	-38.895	1.930	-8.327	7.044	-56.277	1.585	-18.240	19.985
59481.5674	-38.064	2.209	-10.938	2.528	-54.763	1.728	-12.293	20.454
59482.4738	-18.262	1.276	-10.417	0.478	-36.343	3.433	-12.187	21.471
59482.5489	-15.774	1.583	-9.713	2.260	-34.227	0.805	-15.923	13.065
59483.4858	25.655	1.106	-10.094	2.237	6.550	4.117	-19.970	16.203
59483.5546	29.861	1.295	-11.124	4.428	9.043	2.525	-14.453	16.201
59484.4988	65.050	2.025	-9.842	4.994	42.113	3.185	-20.083	21.330
59484.5639	66.129	2.289	-13.077	3.345	40.580	3.190	-19.847	19.379
59485.4748	40.429	2.467	-11.722	5.944	20.773	5.353	-21.977	16.748
59485.5315	37.034	1.510	-11.697	1.733	16.653	3.342	-17.353	17.366
59486.4926	-15.064	2.043	-11.113	3.896	-34.513	2.299	-22.513	16.544
59486.5443	-17.523	2.217	-11.470	3.172	-36.560	4.184	-20.150	15.722
59489.4779	26.808	1.004	-13.587	1.663	6.703	2.669	-17.310	22.572
59489.5321	30.348	1.522	-10.614	2.073	10.307	4.700	-7.510	21.047
59490.5464	64.455	1.441	-12.442	5.035	41.110	4.704	-9.863	13.885
59491.5024	39.454	1.086	-11.777	3.669	18.390	3.772	-20.090	20.410
59491.5537	37.757	0.427	-12.793	3.443	16.627	2.820	-19.893	21.773
59492.4794	-13.074	1.066	-11.642	2.475	-30.050	2.758	-15.573	16.630
59492.5304	-16.533	1.482	-12.559	4.487	-32.950	3.198	-15.593	16.739
59652.8846	88.343	1.307	-36.807	4.940	60.900	4.614	-29.843	2.374
59653.8912	48.766	0.512	-35.059	5.656	25.613	4.774	-35.390	3.549

Table A.1: List of RVs of HD 152246 measured by KOREL and in reSpefo, continued

	KOREL				reSpefo			
RJD	RV_1	σ_{RV_1}	RV_3	σ_{RV_3}	RV_1	σ_{RV_1}	RV_3	σ_{RV_3}
	km.s^{-1}	km.s^{-1}	km.s^{-1}	km.s^{-1}	km.s^{-1}	km.s^{-1}	km.s^{-1}	km.s^{-1}
59653.9103	47.819	1.428	-39.518	4.259	25.350	4.449	-32.897	8.519
59654.8974	-1.930	0.767	-37.575	3.300	-22.050	3.295	-36.013	11.661
59655.8513	-11.497	0.962	-36.160	3.121	-31.683	2.030	-40.340	11.224
59657.7806	61.601	3.598	-39.423	3.197	35.507	2.809	-27.567	1.015
59658.8631	89.530	1.617	-38.880	4.098	59.530	3.075	-35.307	1.594
59659.8575	51.228	1.151	-37.657	2.410	26.280	3.650	-33.617	9.681
59660.8645	-1.779	1.705	-36.414	3.007	-21.750	3.611	-38.300	8.271
59661.8088	-11.556	1.036	-37.482	4.222	-31.337	3.727	-39.840	5.513
59662.8564	16.107	1.518	-34.358	4.404	-4.827	3.756	-33.693	7.218
59662.8951	18.268	1.225	-32.101	3.342	-4.517	2.985	-35.050	11.200
59662.9000	18.297	0.664	-32.923	4.203	-2.113	3.652	-38.480	5.764
59663.8234	62.183	2.083	-34.257	6.177	37.930	4.609	-32.540	5.817
59663.8283	62.281	0.955	-37.421	2.382	36.703	3.939	-35.393	4.837
59664.7933	89.769	2.869	-36.956	3.805	61.233	3.400	-27.763	1.968
59664.7982	88.763	0.833	-36.575	2.373	61.677	3.890	-27.440	6.548
59665.8809	48.963	0.856	-33.632	5.759	25.010	4.928	-30.650	9.398
59666.7188	1.812	2.062	-33.872	1.738	-18.920	2.535	-34.563	8.809
59666.9226	-2.159	0.458	-36.101	4.005	-23.380	2.695	-32.837	9.500
59667.7205	-14.062	0.813	-34.757	2.213	-34.237	3.629	-36.457	9.715
59667.8546	-12.904	0.641	-34.547	2.885	-32.080	2.641	-33.847	10.488
59667.8972	-11.975	1.897	-35.506	1.398	-32.987	2.809	-36.507	10.505
59668.7131	9.005	0.883	-33.943	2.776	-10.723	3.799	-35.037	9.619
59668.8552	15.753	2.693	-33.726	2.391	-5.000	3.287	-36.507	8.661
59668.9009	18.544	3.236	-33.631	5.448	-3.927	2.266	-36.150	10.125
59670.6967	85.527	1.020	-34.566	2.133	59.420	5.154	-30.643	6.422
59670.8657	86.541	2.649	-32.200	5.088	58.323	3.480	-33.027	2.264
59671.7395	53.620	1.005	-34.388	3.532	30.483	3.519	-40.363	10.356
59671.8787	45.865	1.169	-30.945	3.182	24.247	4.376	-38.607	18.123
59672.6979	0.921	0.916	-31.657	2.575	-19.057	2.090	-35.633	15.021
59672.8415	-5.631	2.363	-32.954	3.692	-24.730	1.880	-38.810	15.688
59673.7676	-17.973	1.118	-30.124	2.508	-37.743	2.544	-34.857	15.363
59673.9015	-16.801	0.835	-28.625	1.955	-36.477	1.635	-37.197	19.243
59674.7489	4.091	1.656	-27.623	4.961	-14.680	3.915	-33.773	22.988
59674.8871	9.952	0.908	-27.236	5.102	-9.443	2.684	-36.463	21.320
59675.7583	50.138	1.154	-27.515	3.022	27.800	3.480	-31.477	10.103
59675.8891	55.353	1.310	-26.860	4.580	31.653	2.351	-31.977	11.828
59676.6957	78.852	1.349	-25.591	3.559	53.350	3.895	-31.523	7.216
59676.9010	80.069	1.515	-25.353	2.554	52.443	3.563	-30.790	14.261
59677.6812	48.897	1.857	-22.448	2.376	26.380	2.811	-24.237	9.601
59677.8377	40.754	1.201	-22.267	4.863	18.317	4.320	-27.923	11.736
59678.6757	-6.936	1.442	-21.302	4.305	-25.433	1.753	-26.973	9.587
59678.8252	-12.251	0.840	-23.205	6.655	-30.923	2.898	-30.047	11.938
59679.6737	-27.997	0.866	-19.443	2.179	-44.930	2.187	-26.670	12.163
59679.8504	-29.122	1.095	-19.184	2.164	-47.043	2.232	-27.413	12.937
59680.6747	-10.677	1.138	-15.027	3.579	-28.970	2.407	-20.020	15.469
59680.8918	-3.169	1.294	-14.460	2.466	-22.807	1.744	-19.070	16.401
59681.6709	31.648	1.015	-12.855	1.422	11.877	2.937	-19.467	11.442
59681.8205	38.586	0.554	-11.870	2.617	17.453	4.131	-21.687	14.638
59681.9268	42.815	1.155	-12.796	2.892	22.757	4.922	-18.270	12.455
59683.6821	30.913	2.030	-6.798	3.893	10.073	1.987	-10.360	11.687
59683.8411	22.550	1.273	-3.432	2.817	2.903	1.986	-8.977	16.882
59684.7207	-29.183	0.906	2.157	1.879	-47.230	2.097	-7.670	12.248

Table A.1: List of RVs of HD 152246 measured by KOREL and in reSpefo, continued

	KOREL				reSpefo			
RJD	RV_1	σ_{RV_1}	RV_3	σ_{RV_3}	RV_1	σ_{RV_1}	RV_3	σ_{RV_3}
	km.s^{-1}	km.s^{-1}	km.s^{-1}	km.s^{-1}	km.s^{-1}	km.s^{-1}	km.s^{-1}	km.s^{-1}
59684.8710	-36.376	0.853	2.558	2.010	-52.783	1.520	-10.223	11.730
59685.7188	-54.566	1.180	6.420	2.345	-70.423	2.021	-6.703	12.011
59685.8978	-53.950	0.860	8.736	2.047	-69.233	0.921	-7.767	11.784
59686.7010	-39.654	1.532	14.345	3.696	-54.950	2.086	-0.907	6.117
59686.9267	-32.029	1.423	15.201	1.520	-48.263	4.332	2.423	19.598
59687.7098	0.653	1.496	20.650	1.721	-16.320	2.358	9.710	19.191
59687.9283	9.856	1.142	22.520	4.391	-7.287	3.210	14.360	10.437
59688.7216	26.638	1.180	28.323	2.183	8.283	2.679	18.683	11.920
59690.6545	-65.033	1.191	43.413	4.299	-78.097	1.219	9.950	7.997
59690.8202	-72.610	1.361	46.853	4.690	-85.557	1.866	9.023	6.929
59691.7654	-94.614	1.099	51.262	4.380	-104.063	2.417	7.953	5.579
59692.7713	-79.107	1.209	56.400	4.977	-92.180	3.798	16.757	8.115
59693.7326	-39.348	0.893	65.044	3.744	-54.543	1.091	34.540	9.016
59693.9280	-31.181	0.844	64.869	5.792	-45.233	1.698	38.920	6.769
59694.7521	-10.463	1.315	72.457	5.863	-25.833	1.326	55.333	12.949
59695.7226	-39.292	0.910	75.860	5.052	-51.503	3.430	48.093	9.529
59696.7800	-100.694	1.404	78.426	4.071	-111.910	1.933	30.017	3.279
59700.7971	-18.754	1.322	79.842	4.300	-33.500	2.143	52.873	9.478
59701.9359	-56.551	1.096	77.301	4.172	-67.673	0.241	41.840	8.548
59702.7751	-102.164	1.019	75.268	4.906	-114.693	1.561	23.933	6.151
59703.7477	-120.140	0.953	80.164	3.473	-131.773	0.368	14.227	4.519
59704.7856	-96.758	1.550	75.303	5.849	-106.897	2.688	25.460	13.319
59705.7817	-48.345	2.771	74.499	4.850	-60.693	2.565	42.847	8.392
59706.7325	-14.011	1.455	73.985	3.657	-29.977	1.964	53.103	14.306
59725.6815	-16.657	1.436	53.161	4.275	-31.930	1.123	38.120	13.239
59736.6358	13.068	2.032	42.073	4.086	-3.613	2.223	33.283	20.317
59769.5638	-72.738	1.538	26.841	6.064	-87.023	1.822	3.367	10.423
59769.7800	-72.661	1.099	25.261	4.357	-84.930	2.643	6.703	13.180
59787.4961	-67.850	2.046	20.638	1.900	-79.470	2.548	2.650	9.727
59787.7276	-67.316	1.333	17.652	5.488	-81.053	0.307	-0.047	11.486
59788.5434	-53.277	0.495	17.591	4.352	-69.383	1.158	5.347	14.354
59788.7484	-46.227	0.899	20.493	4.442	-60.270	1.093	4.727	13.294
59789.4897	-13.780	1.531	20.317	2.198	-30.240	2.368	12.900	13.486
59789.6838	-3.068	1.066	19.363	1.951	-19.707	1.062	13.423	13.411
59789.7275	-2.558	1.409	20.544	4.837	-19.347	2.417	8.400	10.462
59791.5489	22.509	1.053	21.010	3.897	4.703	3.624	22.920	17.136
59791.7228	14.979	1.422	18.622	4.019	-2.653	4.206	14.393	11.460
59792.4988	-30.323	1.410	21.863	7.655	-46.527	2.043	8.810	14.527
59792.7160	-41.892	0.634	19.214	2.309	-55.953	1.274	3.927	18.150
59793.5174	-64.491	1.383	17.462	3.346	-77.617	2.120	2.620	9.097
59793.7442	-66.032	0.650	16.699	3.762	-79.083	1.599	0.613	11.937
59818.4774	-49.615	1.634	12.189	3.224	-64.353	2.047	3.253	13.214
59818.6337	-42.528	1.755	11.501	4.079	-59.270	0.731	7.767	17.377
59819.4680	-6.785	1.759	8.747	4.156	-24.890	0.860	10.330	18.939
59819.6385	0.709	0.943	10.281	3.965	-17.027	1.647	6.307	13.025
59820.4667	38.071	3.410	9.490	5.643	17.247	3.881	9.003	14.668
59820.6211	40.853	0.820	13.578	3.871	20.847	3.053	15.613	16.210
59821.5212	32.536	1.485	12.042	1.133	14.130	3.788	7.600	15.504
59821.6512	26.093	1.578	11.766	1.142	6.890	2.314	13.867	18.115
59821.6562	25.642	1.305	12.345	6.134	8.267	3.061	11.470	12.317
59822.5038	-20.824	1.512	9.201	2.079	-38.023	2.494	6.753	16.224
59822.6341	-29.616	0.722	8.477	4.092	-43.767	2.285	2.740	13.222

Table A.1: List of RVs of HD 152246 measured by KOREL and in reSpefo, continued

RJD	KOREL				reSpefo			
	RV_1	σ_{RV_1}	RV_3	σ_{RV_3}	RV_1	σ_{RV_1}	RV_3	σ_{RV_3}
	km.s^{-1}	km.s^{-1}	km.s^{-1}	km.s^{-1}	km.s^{-1}	km.s^{-1}	km.s^{-1}	km.s^{-1}
59824.4903	-46.821	0.462	10.451	1.291	-61.010	1.619	2.097	12.719
59824.6297	-42.620	0.843	10.678	1.095	-56.210	1.642	1.907	10.245
59849.4721	-3.343	2.671	8.439	9.234	-22.527	0.649	-1.460	11.628
59850.4720	41.974	1.398	6.383	5.884	23.133	3.881	6.747	10.000
59851.4841	39.871	1.039	6.104	1.999	20.303	3.930	6.227	10.105
59852.4772	-14.588	0.903	5.248	2.083	-29.977	2.062	3.457	15.757
59853.5696	-52.725	0.665	3.564	4.257	-68.903	1.230	-4.973	13.760
59854.4775	-42.889	0.833	5.676	2.539	-59.403	3.103	0.350	15.929
59855.4778	-1.070	0.904	2.555	2.218	-19.623	1.588	2.333	17.098
59856.4787	43.053	0.675	5.173	1.728	22.463	1.685	9.553	12.418
59857.4786	41.489	0.955	4.947	5.451	21.860	3.618	6.667	11.096
59859.4759	-49.104	0.711	4.793	3.574	-65.043	1.329	-4.953	12.567
59661.0162	-4.668	1.370	-34.755	3.789	-23.107	2.648	-43.433	34.161
59661.1239	-7.384	1.102	-35.318	3.589	-27.717	2.572	-45.730	24.267
59661.1954	-10.522	2.117	-34.487	4.103	-31.323	2.556	-42.860	23.075
59662.0367	-8.366	2.175	-34.038	4.565	-30.110	2.009	-41.117	24.978
59662.1100	-7.702	1.706	-33.570	5.524	-27.980	2.148	-38.637	26.577
59662.1827	-4.255	2.120	-35.034	3.605	-25.700	2.573	-39.487	26.040
59664.0300	70.820	1.323	-35.294	3.850	46.890	5.791	-35.373	18.878
59664.1016	72.950	0.581	-35.486	3.287	46.753	5.086	-35.767	14.686
59664.1735	75.525	0.780	-35.643	3.076	50.333	5.970	-38.753	12.449
59665.0626	85.909	0.933	-35.496	3.240	58.813	5.369	-36.277	15.651
59665.1339	84.124	0.757	-35.402	3.461	56.907	6.453	-40.207	17.087
59666.0586	39.350	1.068	-35.011	3.727	15.983	1.673	-43.597	23.551
59666.1299	35.343	0.672	-35.533	3.369	12.387	1.745	-41.120	21.585
59666.2020	30.036	2.329	-33.603	6.839	9.127	2.081	-40.827	20.814
59667.0120	-6.174	1.307	-35.736	4.428	-26.643	1.317	-44.373	24.941
59667.0842	-8.113	1.499	-34.022	6.279	-29.113	3.421	-40.983	25.213
59667.1753	-8.507	1.135	-35.194	5.133	-27.243	3.436	-42.437	24.269
59667.2169	-9.689	1.522	-34.837	4.315	-30.147	1.501	-46.203	28.085
59669.0304	22.565	1.892	-35.003	3.640	2.077	1.276	-39.983	23.341
59669.1014	25.175	1.195	-32.860	6.040	6.270	1.724	-38.177	24.777
59669.1732	27.932	0.699	-34.114	5.715	7.633	3.669	-44.873	25.273
59669.2259	30.420	0.733	-33.781	3.950	9.427	3.328	-43.310	25.003
59670.9903	84.409	1.173	-35.166	4.138	56.703	4.595	-37.257	18.586
59671.0621	83.467	1.286	-38.251	13.979	56.653	5.116	-33.423	19.403
59671.1399	81.498	1.031	-33.792	4.289	55.110	5.365	-37.740	16.868
59671.2410	78.284	1.707	-32.482	3.546	51.900	5.789	-38.033	15.237
59672.0329	36.411	2.084	-33.151	4.200	12.617	3.506	-38.787	23.756
59672.1038	34.179	1.398	-30.802	6.596	11.510	3.220	-40.313	24.502
59672.1747	30.265	0.691	-32.164	6.218	9.270	4.517	-33.557	21.922
59672.2414	26.620	0.994	-30.346	8.432	5.950	3.565	-36.393	23.737
59673.0095	-9.606	0.873	-31.818	6.940	-29.170	1.811	-37.170	21.766
59673.0812	-11.192	1.033	-32.452	9.378	-31.507	2.982	-38.143	22.098
59673.1526	-12.837	1.562	-32.520	6.420	-34.057	3.502	-39.513	24.148
59673.2182	-13.393	2.237	-33.222	6.345	-34.227	1.666	-39.913	25.465
59673.2402	-13.733	1.501	-32.961	6.704	-33.810	2.180	-42.780	22.744
59682.0038	46.861	2.114	-21.363	12.600	25.560	3.894	-19.127	26.347
59682.0755	48.438	1.454	-20.069	12.270	25.847	4.374	-16.827	23.725
59682.1466	50.593	1.180	-14.388	8.261	28.527	3.386	-13.913	23.641
59682.2227	53.101	1.543	-10.209	3.684	31.257	4.364	-11.347	24.626
59683.0215	60.729	2.295	-11.530	10.123	38.493	5.317	-15.637	30.257

Table A.1: List of RVs of HD 152246 measured by KOREL and in reSpefo, continued

	KOREL				reSpefo			
RJD	RV_1	σ_{RV_1}	RV_3	σ_{RV_3}	RV_1	σ_{RV_1}	RV_3	σ_{RV_3}
	km.s^{-1}	km.s^{-1}	km.s^{-1}	km.s^{-1}	km.s^{-1}	km.s^{-1}	km.s^{-1}	km.s^{-1}
59683.0928	58.441	0.730	-5.238	4.716	36.773	4.979	-10.853	30.872
59683.1639	55.810	2.313	-11.607	13.945	32.573	4.581	-15.360	27.588
59683.2125	54.375	1.914	-6.641	2.683	32.723	4.501	-15.000	26.034
59684.0316	10.682	1.839	-6.367	14.218	-10.327	1.056	-13.510	24.974
59684.1321	2.530	1.931	-6.952	13.791	-17.470	2.419	-11.927	24.973
59684.2030	-0.128	2.169	-9.537	13.866	-21.040	1.463	-12.430	19.092
59684.9555	-38.225	2.239	-3.233	14.434	-57.790	4.047	-12.303	25.005
59686.0566	-52.989	3.736	7.162	9.912	-71.617	1.581	-6.473	20.251
59686.1282	-50.672	3.136	8.554	5.125	-68.670	2.649	-7.670	19.385
59686.1997	-49.949	3.930	8.930	5.527	-67.207	3.056	-5.480	18.785
59686.9933	-27.370	3.297	7.657	20.522	-44.283	1.949	-1.137	22.473
59687.0645	-23.760	3.979	6.885	20.273	-43.647	2.582	1.037	21.912
59687.1357	-19.721	3.200	9.832	12.690	-38.033	2.123	1.973	22.615
59687.2010	-17.540	3.390	9.069	10.624	-36.550	2.264	4.950	26.602
59688.0231	14.456	3.363	12.438	25.063	-5.707	1.957	14.190	35.784
59688.0986	16.570	2.036	18.998	10.737	-2.803	2.756	15.287	27.489
59688.1697	19.530	4.081	21.108	16.783	-0.233	4.773	21.380	26.472
59688.2409	20.765	2.661	19.626	14.354	0.467	1.575	13.883	24.345
59688.9916	24.757	2.507	20.994	21.657	6.427	1.877	25.540	29.656
59689.2186	18.851	2.696	29.406	3.799	0.840	1.809	21.667	25.067

A.2   KOREL solutions of HD 152246

Table A.2: KOREL solutions of orbital parameters for several spectral regions - CHIRON & HERCULES

Short orbit					
Spectral line	T_p (RJD)	e	ω_p (°)	K_1 (km.s^{-1})	$f(m)$ (M$_\odot$)
O II, C III, Si IV	59671.3435	0.0820	37.049	50.87	0.0811
He II 4686	59671.3467	0.0862	37.036	51.40	0.0835
He I 4713	59671.3480	0.0776	37.036	50.62	0.0800
H-beta	59671.3435	0.0820	36.995	50.89	0.0812
He I 4922	59671.3435	0.0820	37.058	51.00	0.0817
He I 5015	59671.3423	0.0862	37.036	51.40	0.0835
He I 6678	59671.3428	0.0866	37.103	51.39	0.0835
interval 4635-5050	59671.3435	0.0820	37.009	51.22	0.0828

Long orbit						
Spectral line	T_p (RJD)	e	ω_p (°)	K_{1+2} (km.s^{-1})	q	K_3 (km.s^{-1})
O II, C III, Si IV	59691.35	0.7529	118.72	54.01	0.983	54.918
He II 4686	59691.82	0.7476	119.61	56.32	0.988	56.975
He I 4713	59691.82	0.7498	119.12	54.56	1.019	53.561
H-beta	59691.32	0.7529	117.85	55.36	1.013	54.632
He I 4922	59691.32	0.7529	118.96	54.31	0.983	55.224
He I 5015	59691.66	0.7476	119.61	56.32	0.988	56.975
He I 6678	59691.60	0.7496	119.49	54.52	0.992	54.960
interval 4635-5050	59691.41	0.7529	118.24	54.98	0.971	56.649

Table A.3: KOREL solutions of orbital parameters for several spectral regions - BESO & FEROS

Short orbit						
Spectral line	T_p (RJD)	e	ω_p (°)	K_1 (km.s^{-1})	dK$_1$/dt (km.s^{-1}.100yr^{-1})	$f(m)$ (M$_\odot$)
O II, C III, Si IV	54285.3582	0.0717	38.41	35.225	0.00266	0.02698
He II 4686	54285.2872	0.0691	37.54	35.054	0.00225	0.02661
He I 4713	54285.1202	0.1806	29.39	36.000	0.00328	0.02762
H-beta	54285.4032	0.1000	39.12	37.258	0.00206	0.03170
He I 4922	54285.2433	0.0569	37.67	35.813	0.00424	0.02844
He I 5015	54285.2298	0.0667	37.00	35.403	0.00306	0.02742
He I 6678	54285.2631	0.0613	37.37	35.670	0.00313	0.02808
interval 4635-5050	54285.2629	0.0835	37.09	35.122	0.00343	0.02668

Long orbit					
Spectral line	T_p (RJD)	ω_p (°)	K_{1+2} (km.s^{-1})	q	K_3 (km.s^{-1})
O II, C III, Si IV	54984.18	117.11	46.93	0.98749	47.53
He II 4686	54985.12	112.86	50.48	0.98999	51.00
He I 4713	54985.80	116.51	54.22	0.99486	54.50
H-beta	54983.11	110.65	52.05	0.98515	52.83
He I 4922	54987.77	106.20	49.34	0.97582	50.56
He I 5015	54985.75	118.59	51.77	0.99020	52.29
He I 6678	54984.53	118.62	59.46	0.99095	60.00
interval 4635-5050	54984.38	118.56	52.99	0.99000	53.53

Table A.4: KOREL solutions of orbital parameters for several spectral regions - FEROS, CHIRON & HERCULES

Short orbit						
Spectral line	T_p (RJD)	e	ω_p (°)	K_1 (km.s^{-1})	dK$_1$/dt (km.s^{-1}.100yr^{-1})	$f(m)$ (M$_\odot$)
O II, C III, Si IV	59671.3435	0.0820	35.62	49.623	0.00234	0.07526
He II 4686	59671.4147	0.0902	37.935	52.29	0.00224	0.08789
He I 4713	59671.4270	0.0910	39.013	51.78	0.00268	0.08531
H-beta	59671.4777	0.1016	39.612	54.81	0.00205	0.10085
He I 4922	59671.4176	0.0896	38.261	51.77	0.00260	0.08530
He I 5015	59671.4165	0.0906	38.476	51.72	0.00268	0.08502
He I 6678	59671.4176	0.0933	38.358	51.53	0.00270	0.08405
interval	59671.3494	0.0892	37.153	50.84	0.00227	0.08080

Long orbit					
Spectral line	T_p (RJD)	ω_p (°)	K_{1+2} (km.s^{-1})	q	K_3 (km.s^{-1})
O II, C III, Si IV	59691.33	119.31	50.62	0.99311	50.97
He II 4686	59692.04	121.98	53.11	0.96000	55.32
He I 4713	59691.96	121.38	52.47	0.97197	53.98
H-beta	59691.91	119.39	54.41	0.98507	55.24
He I 4922	59692.09	122.28	52.81	1.00255	52.68
He I 5015	59692.23	123.03	53.29	0.95078	56.04
He I 6678	59692.22	122.59	52.41	0.95287	55.00
interval	59691.61	118.25	54.37	0.95802	56.75

A.3 Measured radial velocities of Delta Cir

Table A.5: List of RVs of δ Cir determined by KOREL

RJD	RV_1 km.s^{-1}	RV_2 km.s^{-1}	RV_3 km.s^{-1}
54277.5357	39.2625	-36.8483	4.81
54278.539	180.0684	-241.9905	48.0919
54279.5397	-18.4913	109.1623	-37.9747
54280.4974	-127.506	301.1955	-81.7922
54281.489	51.7932	-38.7719	6.5049
54282.4895	177.431	-240.9533	-13.7343
54283.5316	-42.877	109.9217	-38.588
54284.4557	-125.6368	250.9875	-84.3568
54285.5111	80.7686	-100.5679	-37.4037
54286.5221	158.1408	-215.1185	31.945
54298.4795	110.2603	-144.51	-13.9525
54299.4864	-99.5523	223.8232	-15.1975
54300.4761	-84.2348	197.7259	-35.5454
54300.478	-81.229	193.4249	-44.4002
54301.4769	163.1505	-224.2753	-10.7322
54302.4788	93.7964	-112.2786	-32.4701
54660.4716	134.9363	-237.0402	42.0155
54660.4738	135.9848	-226.0923	45.1152
54662.6036	-146.3259	245.4383	5.3741
54663.5894	-60.7482	123.7264	-0.3569
54664.5399	161.779	-288.2429	34.3504
54665.5874	37.7788	-46.8379	20.942
54666.4752	-140.6723	221.8807	27.5865
54667.4791	-64.2112	111.6246	1.4222
54667.5395	-44.3725	83.3758	4.4196
54953.7779	136.2699	-262.9703	50.8356
53403.7712	111.5751	-230.7738	37.7921
55606.7916	-130.7409	123.0177	44.454
55698.7191	178.5662	-260.498	-22.1098
55003.4423	18.4181	-73.809	29.5542
55003.4459	18.7015	-73.9794	29.1579
55004.485	136.3987	-268.0553	22.7716
55004.4911	135.8078	-268.6406	23.0797
55005.7436	-112.4132	160.9599	34.4217
55006.4467	-160.3875	235.6373	17.6164
55006.4502	-160.2382	234.7401	18.5365
55007.4578	45.4655	-124.8717	25.2393
55008.4808	121.6403	-267.3367	20.6381
55009.5609	-103.9655	141.3003	20.1892
55010.4695	-148.6771	226.495	23.5931
55011.6253	110.0414	-228.8505	21.5152
55012.4503	119.7578	-229.1309	19.6478

Table A.5: List of RVs of δ Cir determined by KOREL, continued

RJD	RV_1 km.s^{-1}	RV_2 km.s^{-1}	RV_3 km.s^{-1}
55028.4593	32.1917	-60.7221	24.5892
55028.4614	34.0968	-69.214	4.258
55029.455	-155.6005	211.5262	-30.4572
55029.4576	-155.1843	180.8297	-35.0973
55029.4597	-153.3474	224.6357	-11.701
55029.5212	-157.9948	235.9916	-35.2067
55029.5233	-158.6872	224.4079	-42.0602
55029.5941	-164.244	238.0481	1.9698
55029.6426	-161.6931	238.7408	-7.8336
55029.7319	-165.5683	216.4033	-1.8585
55030.7407	8.9435	-30.5246	52.9846
55030.7428	9.9542	13.9634	15.8773
55030.7456	11.4108	-26.2187	55.5948
55031.478	148.4404	-296.749	1.0657
55360.5334	-60.2724	56.5023	32.6131
55360.5367	-60.2782	58.6347	41.1021
55360.5419	-62.0826	60.3556	33.86
55361.5179	-166.8646	240.2296	42.3703
55364.4855	-71.3876	107.6328	2.932
55365.4824	-159.9005	226.7415	33.8712
55365.4866	-158.4477	240.8287	43.8982
55368.5028	-97.991	123.7983	31.9971
55369.4993	-152.2228	206.9578	1.1008
55379.465	68.626	-169.0003	48.9977
55380.4584	-139.5433	197.6983	8.9959
55382.6147	147.4304	-300.6103	62.6149
55383.727	-10.0502	-105.6807	54.6881
55736.5091	-87.9748	219.3787	-50.9481
55736.5129	-86.4213	192.5187	-71.7509
55737.5351	156.8143	-208.4138	-82.1589
55737.541	161.8209	-214.6525	-53.193
55738.5407	104.4181	-110.8466	-81.1781
55738.5464	106.8304	-112.8839	-50.724
55739.5379	-105.2669	233.2755	-56.2032
55739.5427	-109.1563	241.4754	-11.6831
55740.5354	-61.2985	189.7322	-50.3525
55740.5428	-59.0399	176.1215	-48.4231
55741.5143	170.5621	-233.7981	-103.191
55741.52	176.114	-233.4691	-52.7674
55742.4628	97.9032	-105.8338	-81.399
55742.4783	97.9507	-98.3554	-52.2681
55743.6522	-126.4383	271.2356	-43.0782
55744.5227	-43.0309	144.3322	-50.8165
55744.5294	-46.4584	175.4615	2.6819
55745.4669	177.5929	-242.0627	-52.386

Table A.5: List of RVs of δ Cir determined by KOREL, continued

RJD	RV_1 km.s^{-1}	RV_2 km.s^{-1}	RV_3 km.s^{-1}
55745.4736	181.1747	-221.139	-17.5666
55760.4689	43.7985	-1.976	-17.5157
55760.4734	39.9364	61.0507	-17.0493
55760.493	50.6566	13.6667	-30.6245
55762.466	-12.8555	72.5414	-35.6699
55762.4693	-14.2456	88.9867	-51.1504
56103.4482	-81.0508	130.6501	-106.2823
56103.4539	-86.6478	169.3592	-30.6684
56104.4521	159.959	-250.3541	6.8908
56104.456	156.7635	-249.1905	-17.9156
56105.454	70.9214	-103.3143	-15.2227
56105.4582	67.6081	-101.6498	-39.5122
56106.4571	-126.8089	241.2735	-5.6684
56106.4612	-127.8656	243.1102	-15.6197
56106.4669	-126.9707	243.3479	16.5022
56106.4758	-125.7954	220.0919	-2.8432
56108.4537	169.8413	-264.2109	11.6094
56108.4619	166.1095	-268.3713	-18.4616
56109.4516	49.0847	-70.6649	2.0406
56109.4562	49.7441	-64.4001	-15.2756
56109.4612	48.115	-60.9145	-16.4934
56110.4526	-136.8432	257.2174	-27.921
56110.4599	-138.0302	238.2844	-39.777
56111.4644	-29.6719	86.5531	-11.4318
56111.4711	-25.3446	86.3758	-39.51
56113.4528	35.4406	-74.4238	-30.964
56113.4597	34.7137	-72.234	-42.7752
56132.465	128.9602	-211.4948	0.1201
56133.4631	-82.6498	183.5076	-12.0981
56133.4663	-83.9063	199.8605	6.8885
56133.4706	-84.8901	164.3201	-16.2064
56134.468	-123.4628	227.3561	-11.8172
56134.4759	-122.8763	218.7413	-12.0976
56135.4615	115.6141	-185.232	-12.9351
56135.4683	114.7255	-195.7784	-33.1477
56136.4612	114.4846	-182.6478	-13.5097
56136.4704	110.2221	-197.5	-39.2407
59219.8746	23.3236	-50.8045	-36.1589
59241.8811	131.3699	-203.6131	-27.6476
59251.8905	-133.7932	258.602	13.4793
59253.8629	169.6137	-266.8088	-24.4871
59258.879	24.3735	-21.3905	-104.856
59267.7634	-140.7519	269.6085	4.5362
59276.8782	100.6311	-154.3577	-27.122
59279.8146	-119.5804	264.122	18.6526

Table A.5: List of RVs of δ Cir determined by KOREL, continued

RJD	RV_1 km.s^{-1}	RV_2 km.s^{-1}	RV_3 km.s^{-1}
59286.8022	-117.903	240.1391	35.7736
59290.8611	-137.4652	238.8434	-17.3377
59294.7902	-129.3576	248.6332	-27.2338
59615.8934	-35.2527	54.05	58.2745
59616.9075	164.1374	-290.6183	4.0045
59617.8863	8.3659	-140.1653	32.7899
59618.8802	-144.8759	247.3771	35.7774
59619.9047	-6.4287	17.2399	8.7353
59620.8922	165.5054	-290.5115	5.1986
59620.8957	164.0899	-297.0147	4.3971
59634.8974	-127.2495	230.2016	9.4259
59634.8992	-125.6262	228.4539	29.8447
59635.8231	69.2296	-129.7837	-21.3225
59635.8249	70.4872	-140.9958	-34.64
59636.8661	124.9699	-225.1893	5.9597
59636.8679	123.2368	-223.432	5.6878
59637.8645	-99.5106	158.8166	5.6349
59637.8663	-99.6541	174.551	1.1817
59637.8827	-101.1211	165.1338	5.168
59637.8845	-101.5471	164.3996	4.8697
59638.8726	-125.2286	212.552	36.9793
59639.8509	95.3743	-186.0644	2.6773
59683.6694	132.0296	-240.2717	14.8299
59684.7161	-110.5358	164.613	11.8658
59685.7682	-116.5874	193.2	8.1659
59686.6963	100.2419	-193.0991	2.8087
59687.7052	107.1998	-212.0004	55.2637
59689.7036	-111.6146	185.6041	9.9945
59690.7503	134.3745	-252.0727	13.7903
59691.7154	84.7189	-150.6027	9.1541
59692.7074	-133.7378	212.6862	9.1984